Modeling the transport and optical properties of smoke aerosols from African savanna fires during the Southern African Regional Science Initiative campaign (SAFARI 2000)

R. I. Matichuk,[1] P. R. Colarco,[2] J. A. Smith,[1] and O. B. Toon[1]

Received 18 May 2006; revised 14 September 2006; accepted 2 November 2006; published 18 April 2007.

[1] We investigate the transport and optical properties of smoke aerosols from southern Africa using an offline three-dimensional aerosol transport model. We use Sun photometer retrieved particle size distributions and monthly mean satellite-derived smoke emissions as input parameters. We find that using these observations in our model allows us to reproduce the measured optical properties collected during the Southern African Regional Science Initiative campaign (SAFARI 2000). In particular, we find day-to-day oscillations in the simulated aerosol optical thickness (AOT) similar to Aerosol Robotic Network (AERONET) retrievals, suggesting that variations in aerosol loading are controlled more by transport processes than fluctuations in smoke emissions. We also find that the simulated AOT, Ångström exponent, and single scattering albedo compare well to AERONET. The model and satellite observations from the Moderate Resolution Imaging Spectroradiometer (MODIS) and the Multiangle Imaging Spectroradiometer (MISR) also show that the dominant transport of smoke plumes over Africa was westward during September 2000. However, the satellite observations show higher AOT values than our model over the Atlantic Ocean. These higher values observed by the satellites may be a result of poor single scattering assumptions and the contamination by subpixel clouds in the retrievals. However, the monthly mean smoke emissions may also be too low, resulting in low simulated AOT values. We also find discrepancies between MODIS and MISR, which limit our ability to use the satellite data to validate our model. Our work suggests strategies for improving the treatment of smoke aerosols from African biomass burning in climate and microphysical models.

Citation: Matichuk, R. I., P. R. Colarco, J. A. Smith, and O. B. Toon (2007), Modeling the transport and optical properties of smoke aerosols from African savanna fires during the Southern African Regional Science Initiative campaign (SAFARI 2000), *J. Geophys. Res.*, *112*, D08203, doi:10.1029/2006JD007528.

1. Introduction

[2] Biomass burning is a significant regional and global source of aerosols and trace gases [*Crutzen and Andreae*, 1990; *Hao et al.*, 1990]. The aerosols from both natural and anthropogenic burning of vegetation impact the atmospheric chemistry, the radiation budget, air quality, and carbon cycling in ecosystems. Some of the trace gases emitted from biomass burning fires contribute to the greenhouse effect or are involved in photochemical processes that will generate greenhouse gases [*Crutzen and Andreae*, 1990]. Aerosols produced from biomass burning also influence the radiative properties of the atmosphere. Directly, biomass burning aerosols affect the radiation budget by scattering and absorbing shortwave (solar) radiation. Indirectly, these aerosols can serve as effective cloud condensation nuclei (CCN) which leads to the modification of cloud properties [*Warner and Twomey*, 1967]. *Intergovernmental Panel on Climate Change* [2001] has estimated that the global mean radiative forcing due to biomass burning aerosols is -0.2 W m^{-2} with an uncertainty as large as a factor of 3 and a "very low" level of scientific understanding. Additionally, satellites often observe smoke plumes being transported over intercontinental and continental scales, thereby degrading visibility not only at the smoke source but also downwind of the source [*Annegarn et al.*, 2002; *Stein et al.*, 2003].

[3] Central and southern Africa experience the most extensive biomass burning in the world [*Scholes and Andreae*, 2000]. For this reason, the Southern African Regional Science Initiative 2000 (SAFARI 2000) campaign was devised to study land-atmosphere interactions in southern Africa during the wet season in 1999 and the dry season in 2000 [*Swap et al.*, 2003]. One of the main objectives of SAFARI 2000 was the characterization and quantification of regional emission sources from savanna burning using surface, aircraft, and remote sensing measurements of

[1]Laboratory for Atmospheric and Space Physics, Department of Atmospheric and Oceanic Sciences, University of Colorado, Boulder, Colorado, USA.
[2]NASA Goddard Space Flight Center, Greenbelt, Maryland, USA.

Copyright 2007 by the American Geophysical Union.
0148-0227/07/2006JD007528

aerosol chemical composition, vertical distributions, refractive indices and particle size distributions.

[4] This paper focuses on modeling the transport and optical properties of biomass burning aerosols over southern Africa during the dry season of SAFARI 2000. Since climate models seek to properly represent the properties of such aerosols, one goal of this study is to determine if the data sets provided by the scientific community can be used in climate models to reproduce the observed smoke aerosol optical properties. Our second goal is to better understand the parameters in our model that control the transport and optical properties of these aerosols. We conducted simulations to investigate the model's sensitivity to: the timing and altitude of the smoke emissions; the initial particle size distribution; and microphysical processes, such as coagulation and removal schemes. We also examine the effects different refractive index and humidification assumptions have on its optical properties. To validate the model's performance, we compare our model results to various surface, airborne, and satellite-based measurements collected during SAFARI 2000. The results from this study allow us to develop a set of measurement-based initial conditions to specify the aerosol emissions, injection altitude, and particle size distribution of smoke aerosols in climate models that should be useful for simulating climate responses from smoke plumes. Overall, our work suggests strategies for improving the treatment of smoke aerosols from African biomass burning in climate and microphysical models.

[5] Below, section 2 describes our model and input parameters used to simulate the smoke aerosols in the "base" model. Section 3 presents the base model results, and compares them to observations made during SAFARI 2000. Section 4 presents the results from various sensitivity tests. Lastly, in section 5, we conclude with a discussion of the current ability to successfully model smoke aerosols produced from savanna fires over southern Africa.

2. Model Description

2.1. Aerosol Transport and Dynamical Component

[6] In this study we use an offline three-dimensional aerosol microphysical, transport, and radiation model, which is a version of the Community Aerosol and Radiation Model for Atmospheres (CARMA) developed at NASA Ames Research Center and the University of Colorado [*Toon et al.*, 1988; *Ackerman et al.*, 1995]. Briefly, CARMA is a bin-resolving microphysical model. The aerosol transport and removal processes are handled using dynamical (e.g., pressure, temperature, and wind) and physical fields (e.g., boundary layer mixing diffusion coefficients, convective mass fluxes, and precipitation) provided by the National Center for Environmental Prediction (NCEP) reanalysis package (NCEP/NCAR reanalyses [*Kalnay et al.*, 1996]) and the National Center for Atmospheric Research (NCAR) Model for Atmospheric Transport and Chemistry (MATCH) [*Rasch et al.*, 1997]. Here, the NCEP/NCAR reanalyses are gridded at T63 horizontal resolution (approximately $1.875° \times 1.875°$) with 28 vertical sigma layers extending from the surface to approximately 35 km, and are available each day at 0000, 0600, 1200, and 1800 UTC. The 6-hour meteorological fields generated by the NCEP/NCAR reanalyses and MATCH are linearly interpolated to half-hour time steps in CARMA. For this study, CARMA is run for the period of August and September 2000 at the same temporal and spatial resolution as MATCH but on a limited area grid (180°W to 180°E and approximately 15°N to 60°S).

[7] The microphysical evolution of the particle size distribution in CARMA develops through size specific processes of sedimentation, dry deposition, wet removal, and coagulation. These processes and the coupling of CARMA to MATCH and the NCEP/NCAR reanalyses are discussed in more detail in *Colarco et al.* [2002, 2003a, 2003b, 2004]. The particle size distribution in CARMA is treated using 16 discrete particle size bins spaced logarithmically in radius between 0.01 and 10 μm. We treat the aerosol composition in the model as internal mixtures, where the black carbon (BC) and organic carbon (OC) components of the aggregate are moved together as one particle. The model's advective and diffusive transport processes are calculated using a piecewise parabolic scheme following *Lin and Rood* [1996] which affects each size bin independently. The particle transport by sedimentation and dry deposition is incorporated into the vertical transport following *Pruppacher and Klett* [1997] and *Shao* [2000], respectively. The wet removal (or "scavenging") follows the treatment by *Barth et al.* [2000]. The average residence time of the aerosols given the removal processes in our model is approximately 11 days over southern Africa during September 2000, where about 60% of the total loss is due to dry deposition and sedimentation while the remaining 40% is due to wet removal. The dominant process that controls the coagulation of aerosols in our model is Brownian diffusion [*Toon et al.*, 1988]. Here, the coagulation algorithm preserves the total aerosol volume but decreases the number concentration of particles as the small particles diffuse into larger particles. Coagulation modifies the particle size distribution by increasing the mean radius of the particle size distribution at a rate approximately proportional to the air temperature, the square of the particle number concentration, and the inverse of the particle radius. Although the condensation of gases onto the smoke aerosols does occur in Nature, we do not simulate this process in our model. Since this process occurs immediately after the plume leaves the flame zone [*Reid et al.*, 2004a], we cannot resolve this process in our model using such a coarse resolution. However, given that the initial particle size distribution used in the model is determined from Aerosol Robotic Network (AERONET) retrievals [*Holben et al.*, 1998], which already includes some moderately aged smoke aerosols, we are already incorporating this "near-source" process at the point we emit the aerosols in our model. Additionally, the organic gases that are likely to condense onto the smoke aerosols, such as long chain hydrocarbons, only make up about 10% or less of total aerosol mass [*Andreae and Merlet*, 2001; *Reid et al.*, 2004a]. Therefore these condensable organic gases would have minimal impacts on the total aerosol optical properties.

2.2. Smoke Source Component

[8] The smoke emissions used in the model are interpolated from the Global Fire Emissions Database (GFED), which provides a global $1° \times 1°$ gridded monthly mean map of fire carbon consumption [*van der Werf et al.*, 2003]. The

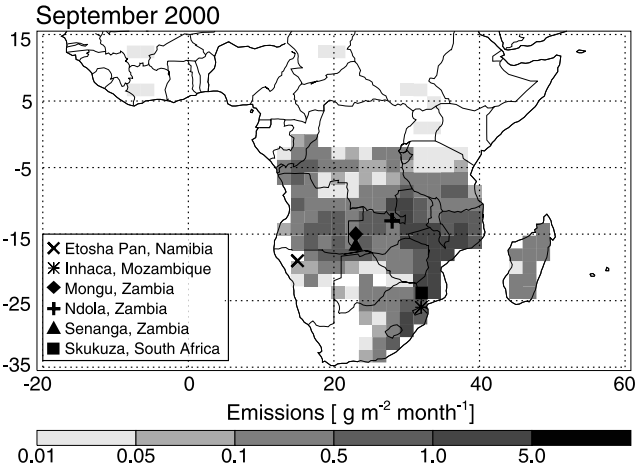

Figure 1. Monthly mean smoke aerosol emissions for September 2000 interpolated from the GFED data set. Also shown are the AERONET sites used for model validation.

variables (e.g., burned area, fuel loading, and combustion factors) used to calculate fire carbon consumed in the GFED are highly uncertain. Of these variables, burned area is probably the most significant for emission estimates and may have an uncertainty of 50% or more over a short time interval over southern Africa [*van der Werf et al.*, 2003]. *van der Werf et al.* [2003] estimate an uncertainty range of greater than 50% for mean annual carbon emission from tropical ecosystems. To convert the carbon consumed because of fires into smoke emissions for our model, we assumed an emission factor of 10.0 (±7.5) g TPM per kg of dry mass [*Sinha et al.*, 2003], which is representative of savanna/grassland vegetation in Africa. We also assume that 45% of the dry mass burned was carbon [*Andreae and Merlet*, 2001]. Given the large uncertainty in the emission factor, we selected a value of 10.0 g TPM per kg of dry mass to use in the base model. The variance in the smoke source function is discussed below in section 4.1.1. We also assume the fires emitted aerosols at a constant rate each day. Over the model domain, which includes the entire Southern Hemisphere, the total smoke emissions are about 4.52 Tg in August and 7.92 Tg in September, where 2.14 Tg and 3.51 Tg of the total emissions were produced over Africa in August and September, respectively. Figure 1 shows the spatial distribution of smoke emissions interpolated to our model grid over Africa for September 2000.

2.3. Smoke Optical Property Calculations

[9] The simulated smoke aerosol optical properties are calculated assuming Mie scattering [*Wiscombe*, 1979] of homogenous aerosols. The optical properties investigated here include the aerosol optical thickness (AOT), Ångström exponent (α), single scattering albedo (SSA), and vertical extinction profiles. In this study, the smoke aerosol is treated as an internal mixture with a density of 1.35 g cm^{-3} [*Reid et al.*, 1998]. We are not partitioning the aerosol into different aerosol species (i.e., BC and OC), but treating the aerosol as aggregated total particulate matter. We also assume a wavelength-independent refractive index (N_{ref} = $1.51 - 0.024i$) that represents the monthly mean refractive index at 440 nm as retrieved by AERONET at Ndola, Zambia, during September 2000 [*Holben et al.*, 1998]. This site was selected because of its proximity to smoke sources, suggesting that it was dominated by locally generated smoke aerosols (Figure 1). Additionally, the humidification of the smoke aerosols is treated in the optical property calculations following a parameterization described by *Magi and Hobbs* [2003]. Briefly, this study found that the aerosol total light scattering coefficient increased with relative humidity without any marked discontinuity during the dry season of SAFARI 2000. In this case, the results can be fitted to an empirical formula, which is a function of relative humidity, the scattering coefficient for the dry aerosol, and empirical fitting parameters based on multiple smoke plume samples over southern Africa.

[10] In the monthly mean optical property calculations, we only include days dominated by smoke aerosols. Our criterion for classifying "smoke-dominated" days is based on an analysis of AERONET climatology of cloud-screened, quality-assured aerosol optical thickness from observations over southern Africa [*Holben et al.*, 1998]. Here we found that the monthly mean AOT at 500 nm [AOT_{500}] exceeded 0.30 during months dominated by biomass burning. Accordingly, when the daily average AOT_{500} retrieved by AERONET was greater than 0.30, the day is classified as smoke-dominated.

2.4. Base Model Description

[11] The input parameters used in the base model are summarized in Table 1. In the base model, we assume the smoke aerosols are represented by a bimodal lognormal size distribution using number fractions (N_f), geometric median radii (r_N), and standard deviations (σ) retrieved by an AERONET almucantar scan at Ndola, Zambia, on 16 September 2000 [*Dubovik and King*, 2000]. We selected this particular particle size distribution because Ndola had the highest daily mean AOT_{500} of all the study sites in the smoke region during September 2000, again suggesting that this site was dominated by locally generated smoke aerosols. Since the average volume size distribution of young smoke plumes (i.e., less than 3 min old) measured by a Passive Cavity Aerosol Spectrometer Probe 100X (PCASP) onboard the UK Met Office, C-130 airplane during SAFARI 2000 [*Haywood et al.*, 2003] had a narrower fine mode (i.e., radius size between 0.01 and 1.0 μm) volume distribution and a lower coarse mode (i.e., radius size greater than 1.0 μm) volume concentration relative to the AERONET retrieval, it is unlikely that the AERONET particle size distribution selected here represents only young smoke aerosols. Rather, these results suggest that the particle size distribution selected for the base model is more likely representative of a mixture of young and moderately aged smoke aerosols, as well as contributions from other aerosols (e.g., dust aerosols), existing in different layers in the atmosphere. However, the coarseness of the model's spatial and temporal resolution prohibits a detailed treatment of truly fresh smoke aerosols. With a grid dimension of approximately 200 km and average wind speeds of 5 m s^{-1} over southern Africa, the smoke aerosols will require about 11 hours to travel across a grid cell. Therefore the Ndola site provides a reasonable compromise between

Table 1. Input Parameters Used in the Base Model

Parameter	Description
Microphysical processes	advection, coagulation, dry deposition, wet removal, and sedimentation
Emissions	emissions: GFED [*van der Werf et al.*, 2003]; emission factor: TPM for savanna/grasslands [*Sinha et al.*, 2003]; assume 45% of dry mass burned was carbon [*Andreae and Merlet*, 2001]
Emission rate over entire model domain	constant throughout
Injection height	mixed between surface and PBLH
Diurnal cycle	aerosol emitted for 12-hour period during daylight hours
Particle density	1.35 g cm^{-3} [*Reid et al.*, 1998]
Initial size distribution	16 bins spaced logarithmically between 0.01 and 10 μm
Mode 1	N_f = 0.99986; r_N [μm] = 0.079; σ = 1.56
Mode 2	N_f = 0.00014; r_N [μm] = 0.695; σ = 2.18
Dependence of size on relative humidity	follows parameterization described by *Magi and Hobbs* [2003]
Refractive index	$N_{ref} = 1.51 - 0.024i$ (applied at all wavelengths)

young and aged smoke aerosols at a scale the model can reasonably simulate.

[12] *Eck et al.* [2003] observed significant diurnal variability in AOT_{500} over six sites in Zambia (Mongu, Ndola, Senanga, Mwinilunga, Zambezi, Solwezi) where the AOT_{500} increased about 25% from 0900 UTC to 1500 UTC. For southern Africa, the Tropical Rainfall Measuring Mission (TRMM) satellite, which makes two overpasses every two days at the equator, also indicated a strong diurnal cycle in fire counts in August and September with a maximum number of fires occurring approximately 3 hours after local solar noon [*Giglio et al.*, 2003]. To represent a diurnal cycle in the base model, the smoke emissions are concentrated during a 12-hour period between 0600 and 1800 UTC. Additionally, the smoke emissions are evenly distributed between the surface model layer and the model layer associated with the top of the planetary boundary layer (PBL) reported by MATCH. On average, the MATCH planetary boundary layer height (PBLH) at the selected study sites peaked at 1200 UTC with heights between 1.50 and 4.00 km.

3. Discussion of Base Model Results

[13] In this section, we compare the simulated optical properties from the base model to satellite, aircraft, and ground-based measurements made over southern Africa during September 2000, and discuss how well the initial input parameters represent the distributions of smoke aerosols near the smoke regions. The model results are compared to data at six sites: Etosha Pan, Namibia; Inhaca, Mozambique; Mongu, Zambia; Ndola, Zambia; Senanga, Zambia; and Skukuza, South Africa (Figure 1). These sites were selected on the basis of the amount of available data

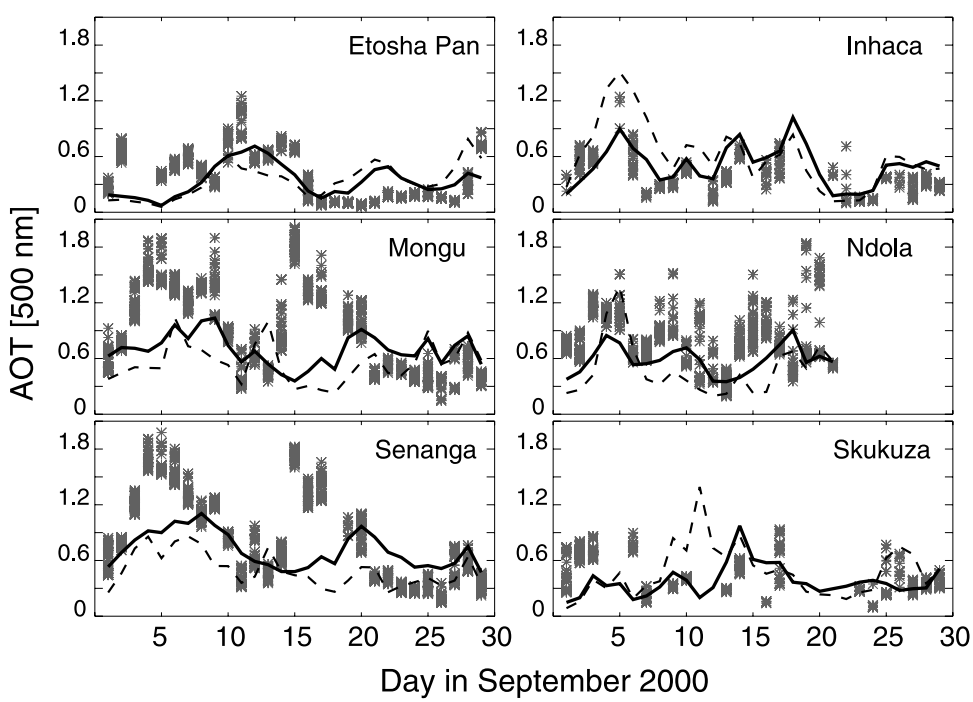

Figure 2. Daily mean AOT_{500} simulated by the base model (solid line) and daily emissions model (dashed line), as well as all AOT_{500} retrievals from AERONET (asterisks) at each study site in September 2000.

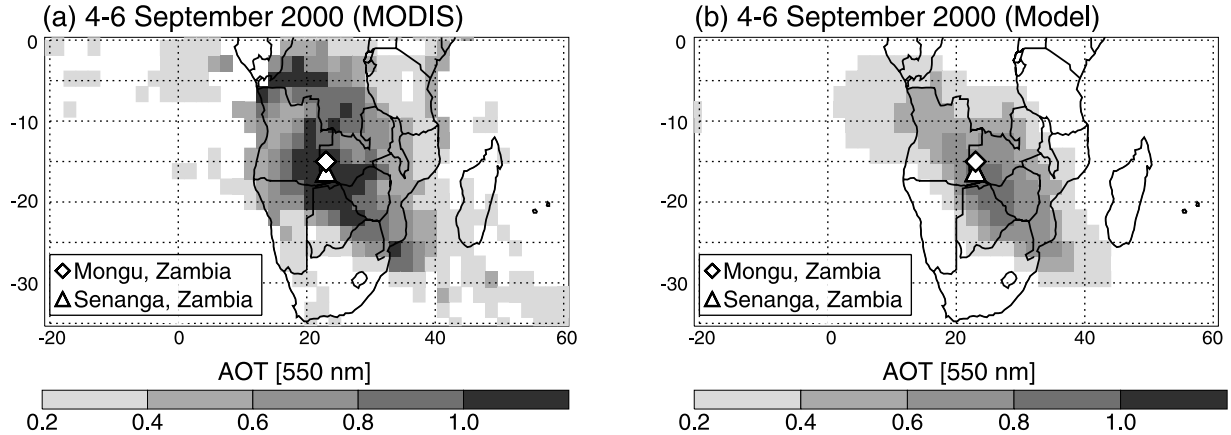

Figure 3. Comparison of mean AOT_{550} (a) observed by MODIS and (b) simulated by the base model during 4–6 September 2000 over southern Africa.

obtained during the SAFARI 2000 campaign and their proximity to the smoke source regions.

3.1. Comparisons to Ground-Based Optical Measurements From AERONET

[14] During SAFARI 2000, there were 17 Sun-sky photometer sites active in southern Africa as part of the globally distributed, federated Aerosol Robotic Network (AERONET) [*Holben et al.*, 1998]. The standardized AERONET instrumentation measures the direct solar beam transmission to determine the column-integrated AOT, and additionally retrieves water vapor, aerosol particle size distributions, and aerosol single-scattering albedo [*Holben et al.*, 1998; *Dubovik and King*, 2000]. In this study, we are using level 2.0 cloud-screened, quality-assured data [*Smirnov et al.*, 2000]. The estimated uncertainty in AOT is ±0.02, which is spectrally dependent with higher errors in the UV [*Eck et al.*, 1999]. The uncertainty in SSA is estimated to be ±0.03. The expected accuracy in the column-integrated volume size distributions is approximately 15–25% for radius sizes between 0.10 μm and 7.00 μm and 25–100% (or less than 10% of $dV/d(\ln r)$ in maximum) for sizes less than 0.10 μm and greater than 7.00 μm [*Eck et al.*, 1999; *Dubovik and King*, 2000].

[15] Figure 2 compares the simulated AOT_{500} (solid black line) to the AERONET retrievals for each day in September 2000 at the six African study sites. The AERONET measurements are essentially point measurements, while the resolution of the model grid is approximately 200 km × 200 km. To make the model and measurements more comparable, we show all the retrievals made by AERONET in a single day and the daily mean AOT_{500} simulated by the base model. Qualitatively, we find that the simulated AOT_{500} falls within the daily range of the AERONET retrievals on most days, and illustrates a similar temporal variation. The day-to-day fluctuations in the simulated AOT_{500} are remarkable given the fact that the emissions used in the base model are released at a constant rate during the month of September. This suggests that the oscillations in the simulated AOT_{500} are controlled more by the variability in the meteorological conditions than the temporal and spatial variations in the fire activity. The importance of the transport dynamics has also been observed by *Myhre et al.* [2003]. On days when the model does not agree with AERONET, the model generally underestimates the daily mean AOT_{500}. However, at Etosha Pan we do find that the model overestimates the daily mean in the latter half of the

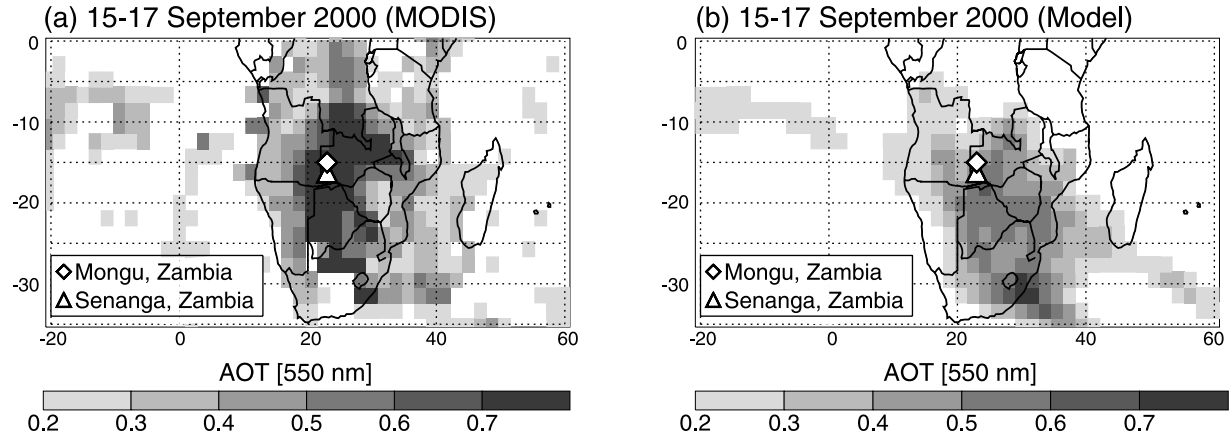

Figure 4. Comparison of mean AOT_{550} (a) observed by MODIS and (b) simulated by the base model during 15–17 September 2000 over southern Africa.

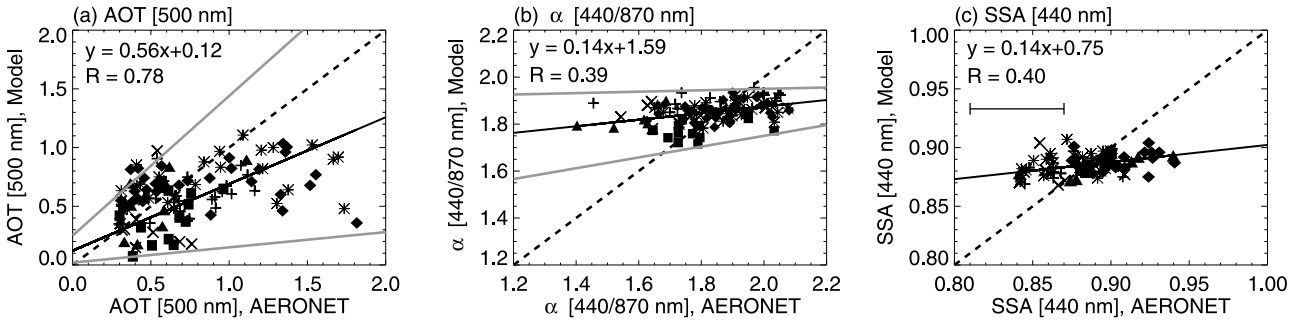

Figure 5. Scatterplots of daily mean (a) $AOT_{500,}$ (b) $\alpha_{440/870}$, and (c) SSA_{440} retrieved by AERONET versus the base model for smoke-dominated days at the six study sites in September 2000. The dashed line represents the 1-to-1 line, and the solid black line represents the line of best fit (LBF) through all points. The equation of the LBF and correlation coefficient (R) are reported. Each study site is represented by a different symbol: Etosha Pan (square), Inhaca (triangle), Mongu (diamond), Ndola (plus sign), Senanga (asterisk), and Skukuza (cross). For clarity, we did not show the uncertainty in the AERONET AOT and α retrievals since they are small. The single bar at the top left in Figure 5c represents the error of ±0.03 in the AERONET SSA retrievals. In Figure 5a, the top gray line represents the LBF in the comparison between AERONET and the double emissions model (y = 1.19x + 0.25; R = 0.98), while the bottom gray line represents the LBF in the comparison between AERONET and the half emissions model (y = 0.13x + 0.02; R = 0.78). In Figure 5b, the top gray line represents the LBF in the comparison between AERONET and the half emissions model (y = 0.03x + 1.89; R = 0.22), while the bottom gray line represents the LBF in the comparison between AERONET and the double emissions model (y = 0.23x + 1.29; R = 0.40).

month, suggesting that the smoke source function is producing more emissions than what actually took place.

[16] We also find that the timing and magnitude in the simulated AOT_{500} compares better to AERONET at Etosha Pan, Inhaca, Ndola, and Skukuza than at Mongu and Senanga. Even though the simulated AOT_{500} does not correlate well with the AERONET observations at Mongu and Senanga, the simulated AOT_{500} at Mongu is well correlated with the simulated AOT_{500} at Senanga. We find a similar correlation between the AERONET AOT_{500} at Mongu and Senanga. Since the two sites are within a couple hundred kilometers of each other (i.e., adjacent grid cells), the similar aerosol loading suggests that these sites were affected by dynamical and emission processes happening on a synoptic scale rather than local scale. Figures 3 and 4 compare the mean AOT_{550} retrieved by the Moderate Resolution Imaging Spectroradiometer (MODIS) [*Kaufman et al.*, 1997; *Tanré et al.*, 1997] to the model during 4–6 September and 15–17 September, respectively. The MODIS retrievals were aggregated to the model resolution using a methodology discussed below in section 3.3. The MODIS results shown in these figures confirm the large-scale aerosol loading, where we find high AOT_{550} values over both of these sites in Zambia, which are presumably associated with biomass burning. Comparing the MODIS observations to the model results reveals that the model underestimates the AOT_{550} during both time periods and places the plume further south during 15–17 September, thereby causing poor correlations between the model and AERONET during this period. Overall, the results shown in Figures 2–4 suggest a problem with the model transport dynamics during these two periods and/or perhaps a major episodic smoke event that cannot be resolved by the monthly mean emissions provided by the GFED data set.

[17] Figure 5 presents scatterplots of the daily mean AOT_{500}, Ångström exponent [$\alpha_{440/870}$], and SSA_{440} simulated by the base model versus AERONET on smoke-dominated days at each study site. In the scatterplot of AERONET AOT_{500} versus model AOT_{500}, we find that the model generally underestimates the daily AOT_{500} by about 50% when the AERONET retrievals are greater than 1.00, even though the model AOT_{500} is well correlated with the AERONET observations (R = 0.78, Figure 5a). Figure 5a

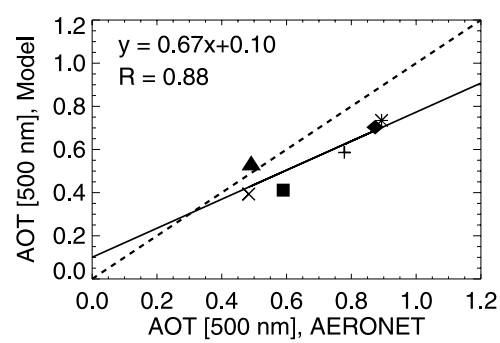

Figure 6. Scatterplot of monthly mean AOT_{500} retrieved by AERONET versus the base model for smoke-dominated days at the six study sites in September 2000. The dashed line represents the 1-to-1 line, and the solid line represents the LBF through all points. The equation of the LBF and correlation coefficient (R) are reported. Each study site is represented by a different symbol: Etosha Pan (square), Inhaca (triangle), Mongu (diamond), Ndola (plus sign), Senanga (asterisk), and Skukuza (cross). For clarity, we did not show the uncertainty in the AERONET AOT retrievals since it is small.

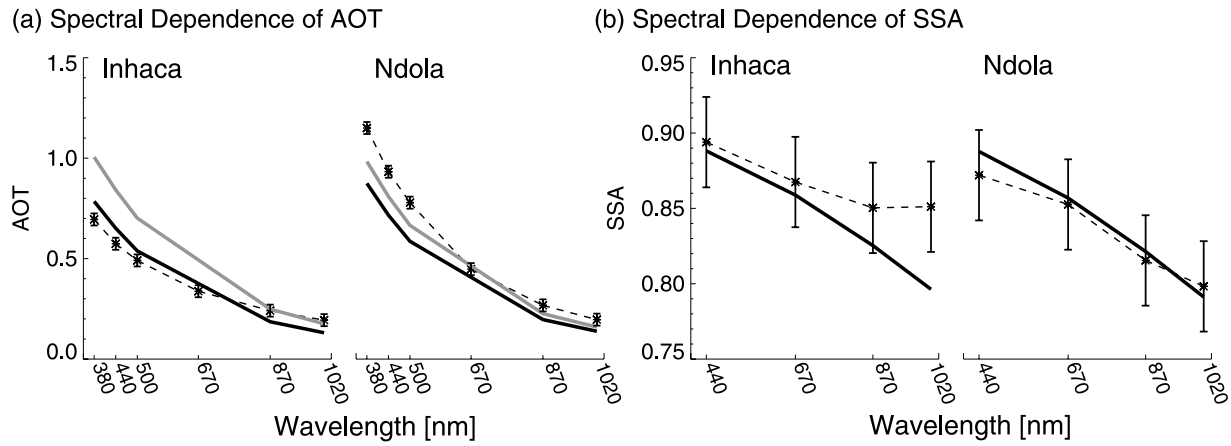

Figure 7. Monthly mean spectral dependence of (a) AOT and (b) SSA retrieved by AERONET and simulated by the model of smoke-dominated days in September 2000 at Inhaca and Ndola. The black solid lines represent the results from the base model, the gray solid lines represent the results from the no wet removal model, and the asterisks connected with a dashed line represent the AERONET retrievals.

may, however, be misleading since we are comparing daily AOT_{500} retrieved by AERONET to daily AOT_{500} derived from monthly mean smoke emissions. Because of the constant emission rate used in the model, the daily fluctuations in the simulated AOT_{500} will be falsely underestimated on days when AERONET observes large AOT_{500} values or individual smoke events. To more accurately represent the results, Figure 6 shows a scatterplot of the monthly mean AOT_{500} of smoke-dominated days simulated by the base model versus AERONET at each study site. We find that the slope of the line of best fit (LBF) increases by about 20%, and the model agrees with the AERONET AOT_{500} retrievals within 30%. In the comparison of daily mean Ångström exponent (Figure 5b), we find that the model results do not show as much variability as the AERONET retrievals. Here the simulated Ångström exponent ranges between 1.70 and 1.95, where the AERONET retrievals range between 1.40 and 2.10. The difference between the model and AERONET suggests that the model is not capturing the variability in the size distribution. In this case, we may not be capturing the age of the smoke aerosols properly, which is expected since the smoke emissions are not time varying. In addition, the spatial resolution of our model may be too coarse to capture any local smoke events. The model results may also be improved if we consider the contribution from other aerosol species that exist at these study sites (i.e., dust, sea salt, and fossil fuel combustion). In the comparison of daily mean SSA_{440} (Figure 5c), we find that the model is within the measurement error of ±0.03 [*Dubovik and King*, 2000]. Note that we do not show scatterplots similar to Figure 6 for the Ångström exponent and SSA since the fluctuations for these optical properties are essentially independent of the smoke emissions.

[18] Figure 7 compares the monthly mean spectral dependence of AOT and SSA retrieved by AERONET to the model results of smoke-dominated days at Ndola and Inhaca for September 2000. At both sites, we find that the mean wavelength dependence of AOT simulated by the model is similar to the wavelength dependence retrieved by AERONET (Figure 7a). The average and maximum difference between the model and AERONET at all measured wavelengths is approximately 15% and 30%, respectively. We also find that the simulated wavelength dependence of SSA is more comparable to AERONET at Ndola than at Inhaca (Figure 7b). At Inhaca, we find that the simulated monthly mean SSA is within the uncertainty of the AERONET retrievals at wavelengths less than 870 nm. However, at wavelengths greater than 870 nm, the model overestimates the absorption by approximately 50%. These results suggest that we are not capturing the variability in refractive index at the larger wavelengths, probably because of the presence of other aerosols, particularly sea salt, at Inhaca. We also find that the SSA decreases as the wavelength increases (SSA is wavelength-dependent) for both the model and the data despite the wavelength-independent refractive index being assumed for the model optical property calculations.

[19] A study completed by *Eck et al.* [1999] suggests that the derivative of the Ångström exponent at multiple wavelengths or curvature term (α') [see *Eck et al.*, 1999, equation (8); *Li et al.*, 1993] provides information about the relative contributions of the fine mode and coarse mode particles to the total AOT. Larger (positive) values indicate relatively larger contributions of fine mode versus coarse mode particles.

[20] Table 2 lists the monthly mean AOT_{500}, $\alpha_{380/440}$, α', and SSA_{440} of smoke-dominated days at Inhaca and Ndola. To compute the derivative of the Ångström exponent (α'), we used wavelengths of 380, 500, and 870 nm. The AERONET observations at both sites show similar Ångström exponent values, but very different curvature values. The slightly lower Ångström exponent and much lower curvature value at Inhaca relative to Ndola is consistent with the known contribution of coarse mode aerosols (i.e., sea salt and dust aerosols) at Inhaca [*Eck et al.*, 1999], while the Ndola observations are more consistent with a site dominated by biomass burning. We also find that the model agrees reasonably well with the AERONET observations at Ndola, but underestimates the coarse mode contribution to the total AOT at Inhaca. The fact that the model underestimates the coarse mode contribution to the total AOT at Inhaca is not surprising since we are not simulating the sea salt and dust aerosols that are present at this site.

Table 2. Monthly Mean AOT_{500}, $\alpha_{[380/440]}$, $\alpha'_{[380/500/870]}$, and SSA_{440} of Smoke-Dominated Days From AERONET and Various Simulations at Inhaca and Ndola in September 2000

Case	AOT_{500}	$\alpha_{[380/440]}$	$\alpha'_{[380/500/870]}$	SSA_{440}
Inhaca				
AERONET	0.49	1.30	0.41	0.89
Base	0.54	1.28	1.31	0.89
Mass	0.78	1.27	1.11	0.82
Ndola				
AERONET	0.78	1.43	1.23	0.87
Base	0.59	1.38	1.24	0.89
Double emissions	1.22	1.26	1.30	0.89
Half emissions	0.26	1.47	1.17	0.86
Mass	0.89	1.27	1.11	0.83
PCASP	0.43	1.66	0.64	0.87
AERONET-mean	0.58	1.46	1.23	0.89
22-bin	0.61	1.32	1.38	0.89
No coagulation	0.55	1.52	1.11	0.88
Density	1.23	1.25	1.27	0.89
Shape	0.58	1.38	1.20	0.89
No dry deposition	0.62	1.35	1.19	0.89
Zhang et al. [2001]	0.56	1.36	1.20	0.89
No wet removal	0.67	1.33	1.26	0.89
WI-*Haywood et al.* [2003]	0.64	1.29	1.36	0.89
WI-AERONET	0.60	1.38	1.31	0.91
WD-AERONET	0.60	1.38	1.21	0.91
WD-AERONET-mean	0.59	1.38	1.15	0.89
No hygroscopic growth	0.54	1.36	1.22	0.88

[21] In the discussion so far, we have focused on Mie scattering calculations to specify the optical scattering and absorption efficiencies at each particle size bin. Alternatively, we could integrate across some portion of the particle size distribution used in the model to arrive at the mass scattering and absorption efficiencies. The mass efficiencies are useful since they are commonly reported from measurements of in situ aerosol optical properties, and they are often used in climate models that do not resolve a particle size distribution to assess the aerosol radiative effect. Table 3 presents the mean mass scattering and absorption efficiencies [m^2 g^{-1}] reported from other studies and this study over Africa. A study by *Formenti et al.* [2003] collected aerosol measurements using various aerosol sampling systems that were onboard the UK Met Office, C-130 aircraft and found mass scattering efficiencies of the fine mode fraction between 4.20 and 4.60 m^2 g^{-1} for smoke aerosols during SAFARI 2000. *Reid et al.* [2004b] used the AERONET data over Zambia between 1995 and 2000 and found mean mass scattering and absorption efficiencies at 550 nm of just the fine mode fraction to range from 3.80 to 4.50 and 0.49 to 0.57 m^2 g^{-1}, respectively. On the basis of the results from the base model, the monthly mean mass scattering and absorption efficiencies at 550 nm over Africa are 3.99 and 0.48 m^2 g^{-1}, respectively. We calculated the monthly mean mass efficiencies by dividing the monthly mean column mass by the monthly mean AOT_{550} of smoke-dominated days at each grid cell and then took the average over southern Africa (i.e., between the equator and 30°S, and 15°E to 40°E). Additionally, the simulated mean mass scattering and absorption efficiencies at 550 nm of just the fine mode fraction over Africa are 4.62 and 0.53 m^2 g^{-1}, respectively. To compare the model results to AERONET, we performed forward calculations based on the monthly mean size distribution and refractive index of smoke-dominated days at Mongu, Ndola, and Senanga retrieved by AERONET during September 2000. We also assumed a particle density of 1.35 g cm^{-3} [*Reid et al.*, 1998]. On the basis of the AERONET retrievals, the monthly mean mass scattering and absorption efficiencies at 550 nm of just the fine mode fraction are 3.91 and 0.49 m^2 g^{-1}, respectively. In general, we find that the model fine mode fraction scattering efficiency is slightly higher than AERONET and the other studies, which may be a result of different particle size distribution, density and refractive index assumptions. Additionally, the model's fine mode absorption efficiency over Africa is slightly higher than AERONET but within the range provided by *Reid et al.* [2004b].

[22] We also find a significant wavelength dependence in the mass scattering efficiencies. In Table 3, the mean mass scattering efficiency over Africa decreases by about 80% from 470 nm to 1020 nm. A similar decrease has been observed by *Reid et al.* [1998], *Eck et al.* [1999, 2001], and *O'Neill et al.* [2002].

3.2. Comparisons of Vertical Extinction Profiles From Airborne and Ground-Based Measurements

[23] During SAFARI 2000, the NASA 14-channel Ames Airborne Tracking Sun photometer (AATS-14) [*Schmid et al.*, 2003], the Cloud Physics Lidar (CPL) [*McGill et al.*, 2003], and the Micro-Pulse Lidar (MPL) [*Spinhirne et al.*, 1995] made measurements of smoke originating from flaming grass fires occurring at several locations in central and southern Africa. In general, these instruments showed that most or all of the aerosols were below 4 km with extinctions between 0.3 km^{-1} and 0.8 km^{-1} at wavelengths near 525 nm during the SAFARI 2000 campaign [*Schmid et al.*, 2003; *McGill et al.*, 2003]. Depending on synoptic conditions, some profiles showed multiple layers, where an aerosol layer would be present between the surface and approximately 1.5 km and an additional layer between 2 km and 4 km [*Schmid et al.*, 2003].

Table 3. Mean Mass Scattering (α_s) and Mass Absorption (α_a) Efficiencies From This Study and Other Studies Over Africa[a]

Reference	Wavelength, nm	α_s	α_a
This study	440/500/550/670/870/1020	5.70/4.70/3.99/2.72/1.54/1.05	0.63/0.54/0.48/0.38/0.27/0.22
This study (fine mode fraction)	550	4.62	0.53
AERONET (fine mode fraction)	550	3.91	0.49
Reid et al. [2004b] (fine mode fraction)	550	3.80–4.50	0.49–0.57
Formenti et al. [2003] (fine mode fraction)	567	4.20–4.60 (±0.60)	

[a]Unit is m^2 g^{-1}.

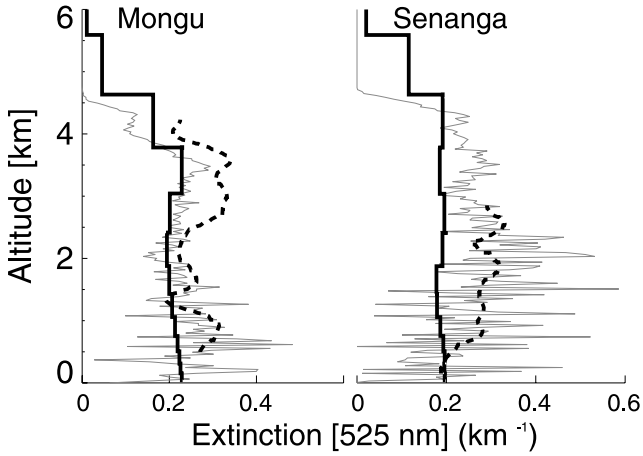

Figure 8. Mean extinction profiles at Mongu and Senanga on 6 September 2000. The CPL profiles are represented by the gray solid lines, AATS profiles are represented by the black dashed lines, and the base model profiles are represented by the black solid lines.

[24] Figure 8 compares the simulated mean vertical extinction profiles at 525 nm to measurements collected by the AATS-14 and CPL at comparable wavelengths (i.e., CPL at 532 nm) at Mongu and Senanga, Zambia, on 6 September 2000. In Figure 8, the mean of the profiles between 0600 and 1200 UTC simulated by the base model is compared to the mean of four CPL profiles measured between 0800 and 1100 UTC and an AATS-14 profile measured at 1000 UTC. In general, we find that the profiles from the model compare well to the observations at the selected African sites. We also find that the profiles at Mongu correlate well with the profiles at Senanga, which is consistent with the comparisons between the model and AERONET AOT_{500} discussed above. The similarities in the observed profiles at these sites further suggest that a large-scale smoke event occurred on this particular day. We do find slight differences between the AATS-14 measurements and the model, where the AATS-14 measurements observed well-defined smoke layers and the model does not. This may be a result of excess mixing in our model. However, it is difficult to draw conclusions about the behavior of the model from single smoke events, such as these aircraft samples, since they may have detected isolated plumes on a scale much smaller than the model resolution.

[25] Figure 9 compares the simulated mean vertical extinction profile at 525 nm from the base model (black line) to the mean MPL measurements (black dashed line) at 523 nm at Skukuza, South Africa. The computed mean includes all days when MPL was operational (i.e., 1–3, 6, 7, 9, 10, 13, 14, and 17 September 2000). In general, we find that the model results compare very well to the MPL measurements.

3.3. Comparisons to Spaceborne Measurements of Aerosol Optical Thickness

[26] Figure 3 shows the mean AOT_{550} retrieved by MODIS and simulated by the base model during 4–6 September 2000. During this time period, the Sea-viewing Wide Field-of-view Sensor (SeaWiFS) observed a significant smoke event, now referred to as the "River of Smoke," where aerosols from biomass burning was transported over southern Africa and the Indian Ocean [*Annegarn et al.*, 2002; *Swap et al.*, 2003]. We find that MODIS and the model produce a similar pronounced aerosol transport corridor across southeastern Africa and over the Indian Ocean. Qualitatively, this simple comparison demonstrates the model's ability to transport smoke aerosols properly on a single day over a large region.

[27] Since the satellite retrievals are available at a much higher spatial resolution than the model (e.g., 10×10 km^2 for MODIS and 17×17 km^2 for MISR), we developed an aggregation and sampling strategy in order to quantitatively compare the satellite retrievals to the model. Briefly, our approach was to first aggregate the highest-quality pixels from the Level 2 products to the model grid, and then calculate the average retrieved AOT_{550}, as well as the number of retrievals available and the standard deviation, in each model grid box on each day. The daily mean AOT_{550} at each grid box was retained as statistically significant when a threshold number of retrievals were made in a given day. The threshold number of retrievals or pixel threshold value is a function of the satellite instrument (i.e., we require more pixels for the high-resolution MODIS and fewer for MISR) and the satellite repeat cycle (near daily coverage for MODIS versus the 7–8 day repeat cycle for MISR). The quality of a retrieval is based on quality assurance flags and other information associated with the retrieval product. The monthly mean at each grid box is then the mean of the daily values passing the pixel threshold, weighted by the number of pixels per day. Finally, the AOT_{550} simulated by the model was sampled near the satellite overpass time and when the satellite daily grid box averages passed the pixel threshold value. Thus, for each satellite we have a unique monthly mean of the model AOT_{550}, which can then be compared to the satellite retrieval at the model resolution.

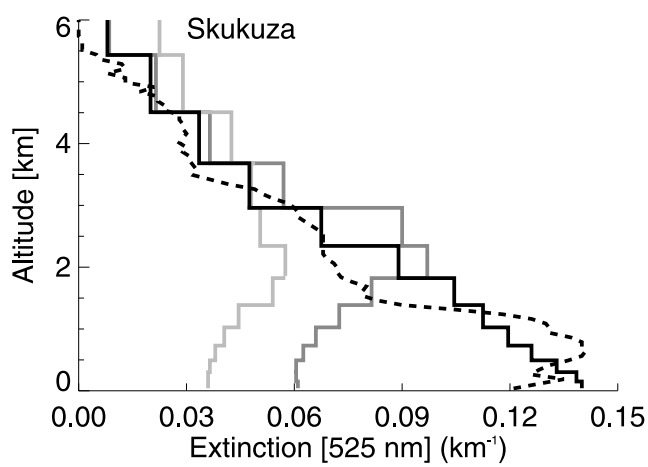

Figure 9. Mean extinction profiles at Skukuza for September 2000. The base model is represented by the black solid line, the three layers model is represented by the light gray solid line, the 2-km-layer model is represented by the dark-gray solid line, and the MPL retrievals are represented by the black dashed line.

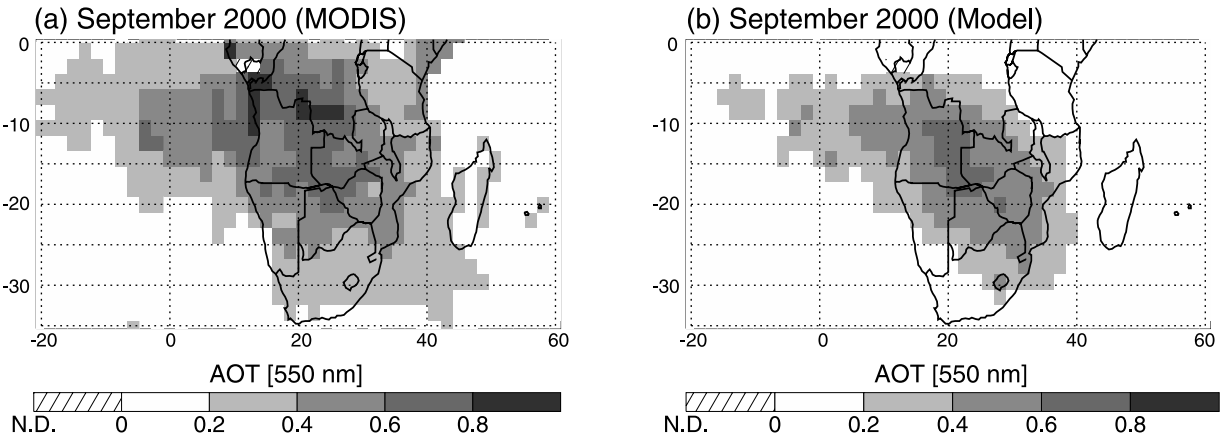

Figure 10. Comparisons of monthly mean AOT_{550} (a) observed by MODIS and (b) simulated by the base model for September 2000 over southern Africa. The hatch marks represent grid boxes with no data (N.D.).

[28] To assess our sampling and aggregation method, we compared our MODIS results to the MODIS Online Visualization and Analysis System (MOVAS) product (http://g0dup05u.ecs.nasa.gov/Giovanni/) and found that the patterns in the monthly mean AOT_{550} are qualitatively consistent between the two products. While we have not fully evaluated this technique, it addresses the nontrivial problem of scaling and aggregating high-resolution satellite observations for quantitative comparisons to relatively coarse resolution simulations. Our work here is ongoing (P. Colarco et al., manuscript in preparation, 2007).

[29] Figures 10 and 11 compare the simulated monthly mean AOT_{550} from the base model to the retrieved AOT_{550} from two polar orbiting satellite platforms: the Moderate Resolution Imaging Spectroradiometer (MODIS) [*Kaufman et al.*, 1997; *Tanré et al.*, 1997] and the Multiangle Imaging Spectroradiometer (MISR) [*Diner et al.*, 1998; *Martonchik et al.*, 1998], respectively, over southern Africa during September 2000. Qualitatively, both satellites show a similar aerosol loading feature over the same portion of southern Africa and the eastern Atlantic Ocean (from approximately 0° to 30°S and 12°W to 40°E). Over land, we find that the peak AOT_{550} observed by the satellites is further north and east (southwestern Zaire) relative to the base model (northeastern Angola). Over the ocean, we find that both satellites detect higher monthly mean AOT_{550} values over the eastern Atlantic Ocean (approximately 5°S to 15°S and 0° to 15°E) relative to the base model. Seeing that the model is misplacing the peak aerosol loading with respect to the satellite observations suggests errors in the biomass burning emissions inventory used in this study or possibly in the model transport dynamics.

[30] Figures 12 and 13 show scatterplots of the monthly mean AOT_{550} simulated by the base model versus MODIS and MISR, respectively. Here we include the same domain shown in Figures 10 and 11, but separate the grid boxes by land and ocean points. This division is particularly relevant for MODIS, which explicitly uses a different inversion algorithm over land than over ocean, but also allows us to compare the performance of MISR over these two different surface classifications. For clarity, we grouped the uncertainty in the data into intervals of 0.20. The error bars in

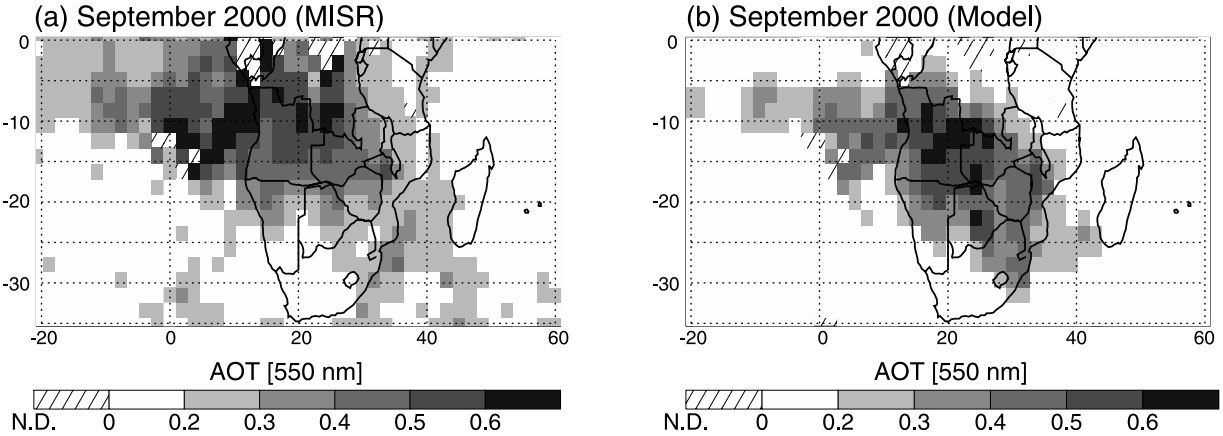

Figure 11. Comparisons of monthly mean AOT_{550} (a) observed by MISR and (b) simulated by the base model for September 2000 over southern Africa. The hatch marks represent grid boxes with no data (N.D.).

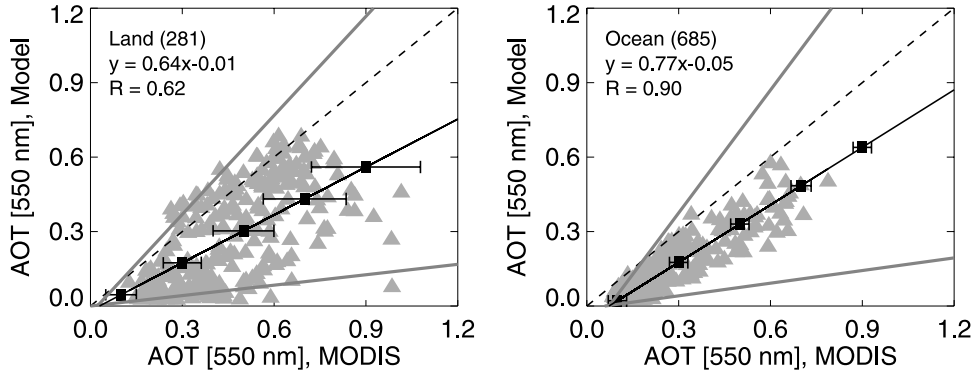

Figure 12. Scatterplots of monthly mean AOT_{550} observed by MODIS versus the base model. The domain is divided into two regions: (left) land and (right) ocean. The dashed line represents the 1-to-1 line, and the solid black line represents the LBF. The equation of the LBF, the correlation coefficient (R), and the number of grid boxes (in parentheses) are reported. The top gray line represents the LBF in the comparison between MODIS and the double emissions model (land: y = 1.33x − 0.03; R = 0.61; ocean: y = 1.65x − 0.12; R = 0.90), while the bottom gray line represents the LBF in the comparison between MODIS and the half emissions model (land: y = 0.14x + 0.00; R = 0.62; ocean: y = 0.17x − 0.01; R = 0.90).

Figures 12 and 13 represent the mean uncertainty in the data at each interval. In general, we find that the model results are linearly correlated to the satellite observations, with stronger correlations over the ocean. Additionally, we find that the model compares better to MISR over land and better to MODIS over the ocean, although the model has lower AOT_{550} values compared to both satellite products.

[31] There are at least three issues that could explain the model's lower AOT_{550} values over the ocean. First, our sampling and aggregation strategy incorporated fewer pixels in a grid box per day over the ocean than land because of sun glint (particularly in MODIS retrievals) and persistent cloud cover in certain regions, so we may be biased in that regard. The average number of pixels in a grid box per day during September 2000 over land was: 107 for MODIS and 48 for MISR; while over the ocean: 84 for MODIS and 40 for MISR.

[32] Second, the model may be deficient in aerosol mass since we are neglecting other important aerosol species, such as sea salt and dust aerosols. The monthly mean Ångström exponent at the 470/670 nm wavelength pair retrieved by MISR and MODIS during September 2000 over the ocean ranged between 0.23 and 1.41. Such low values are commonly associated with large particles, suggesting that dust and sea salt aerosols may be contributing to the higher AOT_{550} values, which would not be seen by the model since we are not simulating these aerosols. In addition, the model smoke emissions may be too low or we may not be properly accounting for significant microphys-

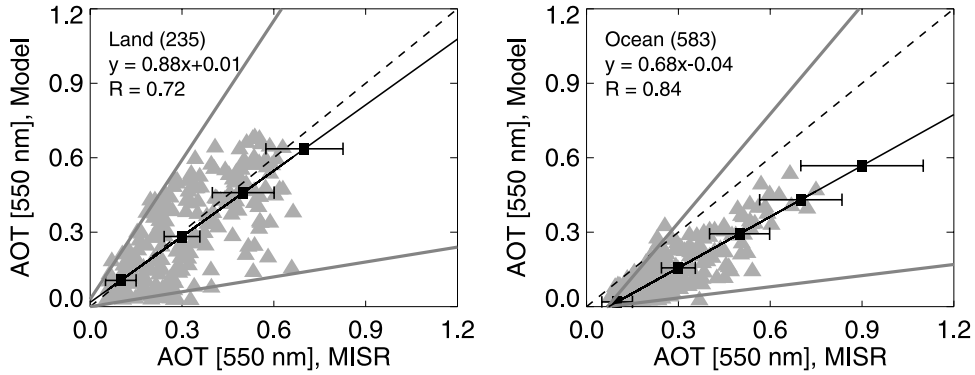

Figure 13. Scatterplots of monthly mean AOT_{550} observed by MISR versus the base model. The domain is divided into two regions: (left) land and (right) ocean. The dashed line represents the 1-to-1 line, and the solid black line represents the LBF. The equation of the LBF, the correlation coefficient (R), and the number of grid boxes (in parentheses) are reported. The top gray line represents the LBF in the comparison between MISR and the double emissions model (land: y = 1.87x − 0.03; R = 0.72; ocean: y = 1.46x − 0.10; R = 0.84), while the bottom gray line represents the LBF in the comparison between MISR and the half emissions model (land: y = 0.20x + 0.00; R = 0.72; ocean: y = 0.15x − 0.01; R = 0.84).

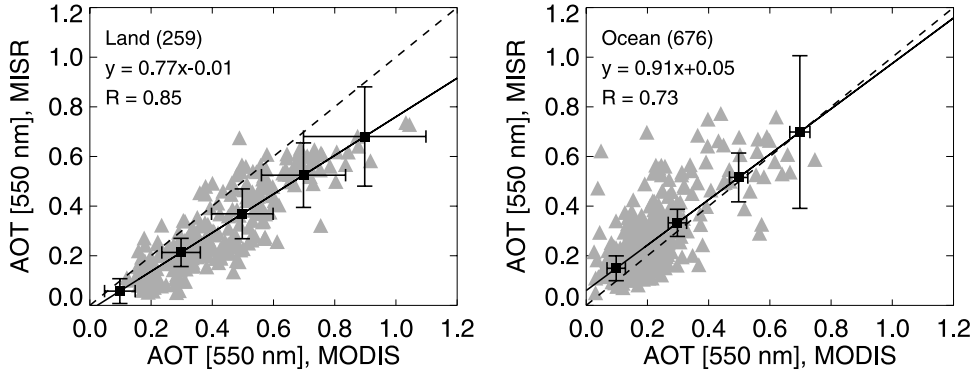

Figure 14. Scatterplots of monthly mean AOT_{550} observed by MODIS versus MISR at points over (left) land and (right) ocean for September 2000. The dashed line represents the 1-to-1 line, and the solid line represents the LBF. The equation of the LBF, the correlation coefficient (R), and the number of grid boxes (in parentheses) are reported.

ical evolution of smoke aerosols through, for example, the humidification of the smoke aerosols.

[33] A third point is that the high monthly mean AOT_{550} values detected by the satellite instruments over the Atlantic Ocean may be due to complications or errors in the satellite retrievals. It is known that this region of the world has persistent, extensive stratus decks. The mean reflectivity from the Total Ozone Mapping Spectrometer onboard the Earth Probe satellite (EP-TOMS) [*Torres et al.*, 1998] during September 2000 indicates high levels of reflectivity (~25% to 50%) over this region, suggesting that unfiltered subpixel clouds may be contributing to the high AOT_{550} feature over the Atlantic Ocean.

[34] Since we observe inconsistencies in the comparisons between the model results and satellite observations, we compared MODIS to MISR. Figure 14 scatters the monthly mean AOT_{550} retrieved by MODIS against MISR at the model resolution. Again, we include the same domain shown in Figures 10 and 11, but separate the grid boxes by land and ocean points. The error bars represent the average uncertainty in the data at each interval of 0.20. In general, we find that the data sets compare well over the land and ocean regions with high correlations, low offsets, and slopes near 1.00. However, MISR is lower than MODIS by approximately 30% over the land region and approximately 10% over the ocean region. The higher AOT_{550} retrieved by MODIS over the land region may be due to an error in the assumed global constant SSA at visible wavelengths in the smoke aerosol retrievals. A study completed by *Ichoku et al.* [2003] suggested that the global constant SSA of 0.90 at visible wavelengths assumed in the smoke aerosol retrievals by MODIS is too high. Rather a SSA of 0.86, or smaller for fresh smoke aerosols, is more representative of biomass burning aerosols over southern Africa. Reducing the SSA would effectively increase the AOT over land. Since we are using the MODIS aerosol product which includes this correction, these results suggest that the correction in the global constant SSA is generating AOT values that are too high relative to MISR.

[35] To better understand the model's performance over land, we compared the simulated mean AOT to MISR, MODIS, and AERONET at the six study sites. Note that the satellite retrievals cannot be compared directly to AERONET since they have been degraded to the model resolution. Direct comparison of the satellite retrievals to AERONET is more correctly done by using the higher-resolution Level 2 products and examining the temporal correlation between the satellite and AERONET observations (e.g., as was done for MODIS by *Ichoku et al.* [2003]). Table 4 shows the mean of all days in September where the MISR, MODIS, and AERONET data sets overlap. Additionally, AERONET and the model are sampled as close to the satellite overpass time as possible. Note that the number of days in September 2000 when all the instruments overlapped was between 5 and 7 days at the selected locations. In general, we find that the model compares better to MISR at four of the six study sites (Etosha Pan, Mongu, Ndola, and Senanga) and compares better to MODIS at the remaining two sites. However, the model is consistently higher than MISR and lower than MODIS. Compared to AERONET, the model is lower at all sites except at Skukuza. Additionally, we find that the AOT retrieved by MISR is always lower than the AOT retrieved by MODIS. From comparisons of the monthly mean optical properties retrieved by AERONET in section 3.1, we found that the optical properties at both Inhaca and Skukuza were different from the other sites since they are influenced by other aerosol sources (i.e., dust and sea salt aerosols). Therefore we find it interesting that the model compares better to MODIS at Inhaca and Skukuza, but better to MISR at the sites that are more clearly dominated by smoke aerosols. Since the model behaves essentially the same at all the sites, this discrepancy in the comparison between MODIS and MISR probably reflects the differences in the retrieval techniques. This relationship suggests that at land sites dominated by fine mode aerosols, presumably smoke aerosols, we might reasonably expect more confidence in the MISR retrievals because of fewer assumptions on the behavior of the surface reflectance characteristics. However, at land sites with multiple sources of coarse mode aerosols, most likely dust and sea salt aerosols, we might expect more confidence in the MODIS retrievals because of its wider spectral range.

[36] Overall, the discrepancies between the MODIS and MISR AOT retrievals over land limit our ability to use the

Table 4. Mean AOT Observed by AERONET, MISR, and MODIS and Simulated by the Base Model at the Six Sites for September 2000[a]

Site	Days	Model [550]	MISR [550]	MODIS [550]	AERONET [500]
Etosha Pan	7	0.38	0.37	0.68	0.51
Inhaca	6	0.36	0.28	0.37	0.38
Mongu	7	0.59	0.54	0.65	0.79
Ndola	6	0.49	0.47	0.62	0.80
Senanga	7	0.60	0.54	0.73	0.75
Skukuza	5	0.46	0.37	0.47	0.30

[a]Note that this mean only includes days when all instruments made retrievals.

satellite data to assess the performance of the model. We do find that the model results are correlated with the satellite observations, suggesting that the differences do not represent random errors, but rather systematic errors. However, the weaker correlations over the land, relative to the correlations found over the ocean, may be due to the variability in the smoke emissions which the model cannot resolve with a monthly mean emissions data set. The better agreement between MODIS and MISR over the ocean and the consistently smaller AOT simulated by the model relative to those sensors may suggest important contributions from other aerosol sources, which are being neglected in the current version of the model, or that our monthly mean smoke emissions are too low. As discussed below, we find that when the smoke emissions are increased by 30%, the base model AOT results are within the error bars of the satellite observations.

3.4. Comparisons to Airborne and Ground-Based Measurements of Particle Size Distributions

[37] Figures 15 and 16 compare the daily mean volume size distribution simulated by the base model to AERONET and PCASP retrievals, respectively, at Etosha Pan on 13 September 2000. The PCASP instrument was onboard

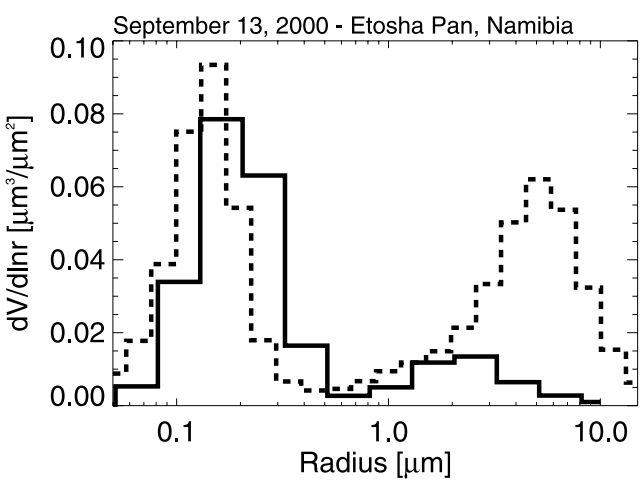

Figure 15. Daily mean column-integrated volume size distribution from the base model (solid line) and AERONET (dashed line) at Etosha Pan on 13 September 2000. The model size distribution is normalized to the fine mode volume concentration of the AERONET retrieval.

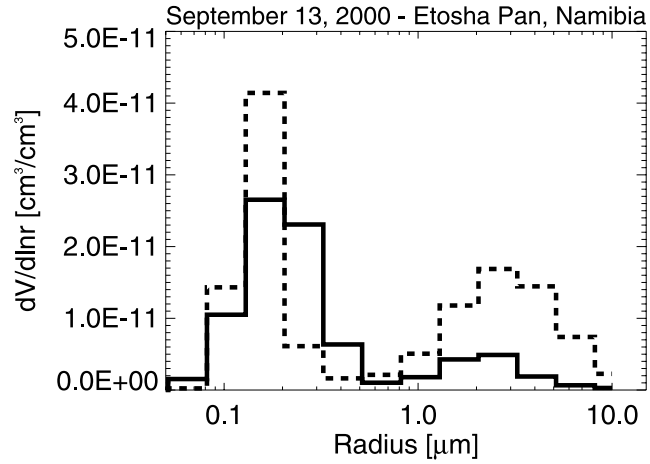

Figure 16. Daily mean volume size distribution from the base model (solid line) and the average PCASP size distribution fit to parameters reported by *Haywood et al.* [2003] (dashed line) at Etosha Pan on 13 September 2000. The model size distribution is normalized to the fine mode volume concentration of the PCASP measurement.

the UK Met Office, C-130 airplane, which flew within smoke plumes at altitudes between 208 m and 1000 m above ground level (AGL) [*Haywood et al.*, 2003]. Compared to AERONET and PCASP, we find that the model has a broader fine mode distribution. This result may be due to the number of bins used to resolve the fine mode fraction in the model (discussed below in section 4.2.1). Additionally, the model has a slightly larger fine mode median radius relative to both observations. Since the PCASP instrument was flown through relatively young smoke aerosols, this measurement may show larger volumes of particles at smaller radius sizes than the model, which was initialized with a particle size distribution representative of young and moderately aged smoke aerosols.

[38] We also find that the simulated volume distribution of particles with radius sizes greater than 2 μm is up to a factor of 5 lower than the AERONET and PCASP retrievals. Assuming that there is no error in the volume distribution of coarse particles retrieved by both instruments, these results suggest that the large particles observed exist at elevated altitudes, and may be transported over long distances. The high coarse mode volume concentrations retrieved by both instruments may also be a result of sea salt and dust aerosols, which are known to influence Etosha Pan. Since we are not simulating these aerosol sources, the model results will not be able to capture the high volume in the coarse mode. However, the model is initialized with much higher volumes of coarse mode particles, suggesting that the model is either removing too many large particles, or we are making incorrect assumptions about the smoke particle properties (i.e., density and shape) which are subsequently removing large particles too quickly (discussed below in section 4.2.3).

4. Discussion of Results From Sensitivity Tests

[39] A series of sensitivity tests are conducted to understand how the assumptions made in the model control the

Table 5. Sensitivity Test Names and Modifications Made Relative to the Base Model

Model Name	Parameter Changed in Base Model	New Parameter Description
Daily emissions	emission rate	GFED emissions linked to ATSR fire counts
Double emissions	emission rate	emitted emissions doubled
Half emissions	emission rate	emitted emissions decreased by half
No diurnal cycle	diurnal cycle	aerosols emitted evenly throughout the day
1500 UTC	diurnal cycle	aerosols emitted at 1500 UTC time step
Three layers	injection height	aerosols emitted in three model layers (1.5 km, 3 km and 5 km)
2-km-layer	injection height	aerosols only emitted in one model layer (2 km)
Mass	size distribution/optics	partitioned aerosol mass and computed optical properties following *Chin et al.* [2002]
PCASP	size distribution	applied N_f, r_N, and σ reported by *Haywood et al.* [2003] for fresh smoke aerosols
	Mode 1	$N_f = 0.9957$; $r_N = 0.10$ μm; $\sigma = 1.30$
	Mode 2	$N_f = 0.0041$; $r_N = 0.22$ μm; $\sigma = 1.50$
	Mode 3	$N_f = 0.0002$; $r_N = 1.00$ μm; $\sigma = 1.90$
AERONET-mean	size distribution	applied N_f, r_N, and σ representative of monthly mean data of smoke-dominated days reported by AERONET at Ndola, Zambia
	Mode 1	$N_f = 0.9999$; $r_N = 0.08$ μm; $\sigma = 1.53$
	Mode 2	$N_f = 0.0001$; $r_N = 0.73$ μm; $\sigma = 2.17$
22-bin	size distribution	22 size bins spaced logarithmically between 0.05 and 15.00 μm
No coagulation	microphysical process	no coagulation
Density	density of particle	density: 0.675 g/cm^3
Shape	shape of particle	particle shape: flat plates
No dry deposition	microphysical process	no dry deposition
Zhang et al. [2001]	microphysical process	dry deposition routine from *Zhang et al.* [2001]
No wet removal	microphysical process	no wet removal
WI–*Haywood et al.* [2003]	refractive index	$N_{ref} = 1.54 - 0.025i$ (wavelength-independent)
WI-AERONET (16 Sep 2000 at Ndola)	refractive index	$N_{ref} = 1.52 - 0.019i$ (wavelength-independent)
WD-AERONET-mean (Sep 2000 mean RI at Ndola)	refractive index	uses wavelength-dependent refractive indices
	380 nm	$N_{ref} = 1.51 - 0.024i$
	440 nm	$N_{ref} = 1.51 - 0.024i$
	670 nm	$N_{ref} = 1.52 - 0.020i$
	870 nm	$N_{ref} = 1.53 - 0.020i$
	1020 nm	$N_{ref} = 1.54 - 0.016i$
WD-AERONET (16 Sep 2000 mean RI at Ndola)	refractive index	uses wavelength-dependent refractive indices
	380 nm	$N_{ref} = 1.52 - 0.019i$
	440 nm	$N_{ref} = 1.52 - 0.019i$
	670 nm	$N_{ref} = 1.52 - 0.016i$
	870 nm	$N_{ref} = 1.53 - 0.017i$
	1020 nm	$N_{ref} = 1.53 - 0.016i$
No hygroscopic growth	relative humidity	assumed relative humidity is zero

simulated results. We partition these tests into two basic divisions. First, we consider a series of tests exploring the model's sensitivity to the smoke source function, the diurnal variability in the smoke emissions, and the injection altitude of smoke emissions (section 4.1). Second, we consider a series of tests exploring the model's sensitivity to various assumptions about the particle microphysics, including initial particle size distribution, aging, removal, and particle optics (section 4.2). Each test is assigned a name, and a summary of the names and variances in each test are presented in Table 5.

4.1. Sensitivity of the Smoke Source Function

[40] In this section, we investigate the model's sensitivity to daily and monthly emissions data sets (section 4.1.1), the diurnal variability in the smoke emissions (section 4.1.2), and different smoke emission injection altitudes (section 4.1.3).

4.1.1. Sensitivity to Daily and Monthly Aerosol Emissions

[41] An issue with using the GFED carbon emissions is that it only provides monthly mean carbon emissions. An emissions inventory with a finer temporal resolution may be important for realistically specifying the temporally varying smoke aerosol optical properties. Therefore, rather than constantly emitting the same amount of smoke throughout the month, we generated smoke emissions that fluctuated day-by-day. The fluctuating daily smoke emissions were constructed by correlating the emissions provided by the GFED to the Along Track Scanning Radiometer (ATSR) daily hot spot data [*Arino et al.*, 1995]. Here, we aggregated the daily ATSR hot spots to the same grid used in the model and the emissions source. The daily emissions for each grid cell were found by multiplying the monthly total smoke emissions from the grid cell by the fraction of the monthly total fires occurring in the grid cell on that day. Potentially this underestimates the number of days on which our fires are active because heavy cloud or aerosol cover may mask fire hot spots that would otherwise be identified. On the other hand, the coarseness of the model grid might alleviate this problem so that in an average sense the day-to-day variability of fires occurring in the grid cell is about right. We note that the monthly mean emissions provided by the GFED data set were constructed using the TRMM fire counts. However, we cannot use the TRMM fire counts here because of its irregular repeat cycle over a given region, which would cause it to sometimes miss a day

entirely. In the monthly average sense, TRMM may be more useful because it sees more of the diurnal variability in emissions. We also note that we cannot use MODIS fire counts in this test because of problems with the MODIS detectors associated with hot spot detection during this time period (http://modland.nascom.nasa.gov/cgi-bin/QA_WWW/qaFlagPage.cgi?sat = terra).

[42] In Figure 2, we compare the AOT_{500} results from a model simulation using this daily emissions data set (referred to as "daily emissions" in Table 5) to the base model and AERONET retrievals. This comparison shows that fluctuating the smoke emissions does have some impact on the day-to-day variability in the aerosol loading, particularly at Mongu, Ndola, and Skukuza. However, in some cases, the AOT_{500} comparison between the daily emissions test and AERONET is worse, suggesting that simply using hot spots to scale the gridded GFED emissions may miss important variables that determine the actual day-to-day emissions, such as the size of the fire, the type of vegetation burned, or the diurnal cycle of emissions. Furthermore, the daily emissions cannot be used to explain the missing aerosol in the model in mid-September at Mongu or Senanga, suggesting that there is either a missing source in the GFED or the model transport dynamics is somehow incorrect in this region at this time. Still, the daily emissions case and the base model are more similar than they are different, suggesting that the variation in the number of fires and timing of the fires throughout the month are not as important as the variability in the meteorological conditions for the local AOT_{500}. The development of a daily emissions data set that considers more details about the smoke sources is a subject of future research.

[43] Given that the combined uncertainty in the GFED carbon emissions and emission factor can be about a factor of 2, we conducted two additional simulations where we doubled and halved the emissions in the model. These simulations are referred to as "double emissions" and "half emissions" in Tables 2 and 5. Figures 5, 12, and 13 show the LBF from the comparisons between the observations and these two test cases. The top gray line represents the LBF from the comparison between the double emissions model and the observations, while the bottom gray line represents the LBF from the comparison between the half emissions model and the observations in all figures except in Figure 5b, where the LBF are reversed. In general, we find a linear relationship between the smoke mass emitted and the simulated AOT (Figures 5a, 12, and 13). Relative to the base model, we also find that the monthly mean AOT_{500} at Ndola increases/decreases by about a factor of 2 when the emissions are increased/decreased by a factor of 2 (Table 2). Thus, in order for the simulated AOT to be within the error bars of all the observations (i.e., MODIS, MISR, and AERONET), we find that the smoke emissions in the base model will have to increase by about 30%. In Ångström exponent comparisons between the base model and the two emissions tests, we find that increasing/decreasing the emissions by a factor of 2 decreases/increases the mean Ångström exponent by approximately 10% (Figure 5b and Table 2). The changes in the simulated Ångström exponent are due to impacts from coagulation in the model. By increasing the amount of smoke aerosols, we are essentially increasing the rate of coagulation, thereby increasing the median radius of the particles. Additionally, we find that the monthly mean curvature values and SSA_{440} at Ndola are relatively insensitive to changes in the smoke emissions. Overall, the uncertainty in the smoke source function used in this study has significant impacts on the simulated AOT, but small effects on the other simulated optical properties.

4.1.2. Sensitivity to the Diurnal Cycle of Aerosol Emissions

[44] As pointed out earlier, *Eck et al.* [2003] reported diurnal variability in the AOT_{500} retrieved by AERONET at sites in Zambia during SAFARI 2000. In general, this study found that the AOT_{500} increased about 25% from 0900 UTC to 1500 UTC at the sites in Zambia. This may be a result of real diurnal patterns in the fires themselves, in which case the observations are seeing the plumes from nearby sources. The diurnal variability may also reflect the aerosol response to humidity or venting from the planetary boundary layer. In the base model where the particles were injected between 0600 UTC and 1800 UTC every day, we found a very weak diurnal cycle in the simulated AOT_{500} at the individual AERONET sites. The simulated mean AOT_{500} increased about 10% from 0600 to 1800 UTC at the six sites. Since we did not observe a strong diurnal trend in the base model, we conducted two additional tests where we varied the timing of the emissions throughout the day. In one sensitivity test, we relaxed the base model diurnal cycle (referred to as "no diurnal cycle" in Table 5) by evenly distributing the smoke emissions throughout the day. In another test, we injected all the smoke at the 1500 UTC time step on each day (referred to as "1500 UTC" in Table 5). Relative to the base model, changing the diurnal cycle of the smoke emissions only had small effects on the model vertical extinction profile at the lowest altitudes (between 0.00 and 0.50 km) and almost no effect above that. Additionally, the simulated mean AOT_{500} for both test cases increased 10% or less from 0600 to 1800 UTC at the six sites. In the test where nocturnal emissions were allowed, these results suggest that those emissions can stay near the surface at night, but are quickly mixed throughout the boundary layer during the day. Overall, we are unable to reproduce the diurnal variability in AOT observed by *Eck et al.* [2003]. Changes in the smoke morphology, perhaps from daily variations in humidity, does not seem likely as our computed smoke aerosol optical properties agree reasonably well with the observations available. Therefore it seems more likely that AERONET is more sensitive to very local sources which are dispersed quickly in our grid.

4.1.3. Sensitivity to Aerosol Injection Height

[45] To test the model's sensitivity to the altitude at which the smoke emissions are initially distributed vertically above the source regions, we ran two additional simulations that were based on information provided from the literature. During SAFARI 2000, trace gases and aerosols over the subcontinent were consistently observed as trapped stable layers at approximately 850 hPa (~1.5 km), 700 hPa (~3.0 km), and 500 hPa (~5.5 km) within the lower troposphere [*Stein et al.*, 2003; *Schmid et al.*, 2003; *McGill et al.*, 2003]. The injection altitude of smoke emissions was assumed to be associated with buoyancy generated by the release of heat in the fires, and the amount of heat release was found to be dependent on the amount and type of vegetation being burned, and whether the combustion was

smoldering or flaming [*Andreae and Merlet*, 2001]. Using this information, we ran one simulation with the smoke emissions centered at three model layers and referred to as "three layers" in Table 5 (layers included: 1.42 km (0.41 km thick), 3.06 km (0.67 km thick), and 5.64 km (0.98 km thick)). In another simulation, we emitted the smoke emissions within one model layer, centered at 2.42 km (0.58 km thick) and this test is referred to as "2-km-layer" in Table 5.

[46] We find that when the PBLH is higher than the altitude at which we emit the smoke emissions, the smoke aerosols are quickly mixed within the PBL, generating vertical extinction profiles that are almost uniform with altitude. At Mongu and Senanga, where the monthly average PBLH provided by MATCH is approximately 4 km, we find that the profiles from the three layers model and 2-km-layer model are similar to the base model results in Figure 8. However, when we emit the smoke aerosols above the PBLH, we find that the model is capable of maintaining a smoke layer. At Skukuza where the monthly average PBLH is approximately 2 km, we find that the profiles from the three layers test and 2-km-layer test are not similar to the base model (Figure 9). Instead, the smoke appears to reside at an elevated altitude relative to both the base model and the observations. Overall, the base model of uniform mixing throughout the depth of the PBL is the most comparable to the observations.

4.2. Sensitivity of Simulated Aerosol Properties to Microphysical Processes

[47] In this section we discuss the implications and limitations of the modeled smoke aerosol properties to various assumptions made about the aerosol microphysics, including choice of initial particle size distribution and resolution of bin sizes (section 4.2.1), aerosol aging (section 4.2.2), aerosol removal processes (section 4.2.3), and aerosol optics (section 4.2.4).

4.2.1. Sensitivity to Treatment of Particle Size Distribution

[48] CARMA is a bin-resolving cloud and aerosol microphysics module. Incorporation of such a module into a large-scale transport-modeling framework can easily become computationally prohibitive. To reduce this computational expense, CARMA can be adjusted to use the fewest number of size bins and microphysical processes necessary to carry out a given problem. In contrast, a more typical chemical transport model undertaking the problem we presented here might have a greatly reduced aerosol microphysical modeling capability compared to CARMA. As an example, the NASA Global Ozone Chemistry Aerosol Radiation and Transport (GOCART) model [*Chin et al.*, 2002] neglects the explicit treatment of aerosol particle size distributions for carbonaceous particles and instead partitions the aerosols into hydrophobic and hydrophilic OC and BC components. The subdivision of the aerosol mass to hydrophilic and hydrophobic components affects the aerosol optics, as well as the aerosol lifetime since only the hydrophilic fraction is scavenged by precipitation. The timescale for conversion of hydrophobic to hydrophilic aerosols in these models is typically short (approximately 1–2 days) and is intended to represent the condensation of gases and water absorption onto the particles, but does not allow for explicit treatment of other aging mechanisms, such as coagulation or the treatment of the aerosol optics as internal mixtures. On the other hand, it should be pointed out that GOCART is more complete than our model in the sense that it treats all major tropospheric aerosols species.

[49] To understand the uncertainty in the prescribed initial particle size distribution used in the model, we consider how many size bins are required to adequately constrain our problem. On the basis of earlier simulations [e.g., *Colarco et al.*, 2004], we chose to use 16 size bins (referred to as "16-bin" hereinafter) spaced logarithmically in radius between 0.01 and 10.00 μm in the base model. As a limiting case, we also considered a case with 22 size bins (referred to as "22-bin" hereinafter) spaced logarithmically in radius between 0.05 and 15.00 μm, which is identical to the bin separation AERONET uses to report their size distributions. Using the wavelength-dependent refractive index and particle size distribution retrieved on 16 September 2000 at Ndola, we compute the Ångström exponent for the 440 and 870 nm wavelength pair ($\alpha_{440/870}$) and curvature term at 380, 500, and 870 nm wavelengths ($\alpha'_{380/500/870}$) for the 16-bin and 22-bin cases, and then compare the values to the AERONET observation on this particular day. We find that the $\alpha_{440/870}$ on 16 September is 1.93, 1.97, and 1.96, respectively, for the AERONET observation, 16-bin case, and 22-bin case. Additionally, the curvature terms on this day are 1.21, 1.03, and 1.12, respectively, for the same three cases. The computed Ångström exponents are nearly identical to the observed AERONET value. On the other hand, compared to AERONET, the computed curvature terms are approximately 20% and 10% smaller in the 16-bin case and 22-bin case, respectively. Note that the curvature term was defined in terms of the 380, 500, and 870 nm wavelengths, and of those three wavelengths AERONET only retrieves refractive indices at 870 nm. Therefore we interpolated the 500 nm refractive index from the 440 and 670 nm retrieved values. Additionally, the 380 nm refractive index is assumed to be the same as the 440 nm retrieved value, which seems to be a reasonable assumption based on the discussion by *Torres et al.* [2005].

[50] The discrepancy in the computed curvature terms above can be attributed to the number of size bins used to resolve the fine mode fraction of the particle size distribution. We note that there is essentially no contribution to either the Ångström exponent or curvature term from particles with radius sizes smaller than 0.05 μm or larger than 10.00 μm. The fine mode particle scattering area is primarily at radius sizes between 0.05 and 0.60 μm, which comprises six size bins in the 16-bin case and nine size bins in the 22-bin case. From sensitivity tests with more bins, we find that increasing the number of size bins in the fine mode improves the accuracy of the computed optics. Here the accuracy of the computed optical properties converges when ten or more size bins are used in the fine mode particle size distribution. The improved accuracy of the optics by adding more size bins is also illustrated in the comparison of the $\alpha_{380/440}$ using the refractive index and particle size distribution retrieved on 16 September 2000 at Ndola. On this particular day, we find that the $\alpha_{380/440}$ is 1.48, 1.52, and 1.47, respectively, for the AERONET observation, 16-bin case, and 22-bin case.

[51] In the following discussion, we have considered the effects of changing the number of size bins and the initial size distribution relative to the base model. Our simplest sensitivity test is called the "mass" model. In this case, we integrated the mass across all the size bins in the base model and computed the aerosol optical properties following *Chin et al.* [2002], assuming the smoke aerosol was externally mixed, where the mass was partitioned into BC and OC, and completely hydrophilic because of the short timescale for conversion. We also consider different assumptions about the initial particle size distribution based on the retrievals by AERONET (column-integrated) or measurements made by the airborne PCASP instrument (in situ) [*Haywood et al.*, 2003] over smoke source regions during the SAFARI 2000 field campaign. In the "PCASP" model, we used a particle size distribution that was fit to parameters determined from mean PCASP observations taken within a smoke plume at Otavi, Namibia, on 13 September 2000 [*Haywood et al.*, 2003]. The "AERONET-mean" model used a particle size distribution that was fit to the mean parameters of smoke-dominated days retrieved at Ndola, Zambia, by AERONET during September 2000. The "22-bin" model resolves the particle size distribution using the AERONET reported bins as described above. Table 5 lists the model names, input parameters that were changed in each model, and the number fractions, geometric standard deviations and median number radii associated with each particle size distribution.

[52] Table 2 lists the monthly mean AOT_{500}, $\alpha_{380/440}$, α', and SSA_{440} of smoke-dominated days for selected sensitivity tests at Ndola and Inhaca. Note that not all of the results are shown at Inhaca since they show the same conclusions as at Ndola. In general, we find that the simulated mean AOT_{500} and SSA_{440} are the most sensitive to the mass and PCASP parameterizations. Compared to the base model, the mean AOT_{500} of the mass model is approximately 50% higher at both study sites. These results are expected since the mass model implicitly assumes that all the smoke is in the fine mode, which has greater aerosol extinction per unit mass than the coarse mode. However, the low monthly mean Ångström exponent (α = 1.27) of the mass model at both sites suggests that its assumed fine mode particle size distribution has a slightly larger median radius than the base model or observations. We also find that the mass model is approximately 50% more absorbing than the base model at both study sites. This is expected since the imaginary part of the refractive index assumed for organic carbon, which makes up approximately 90% of the smoke mass, is much more absorbing relative to the base model.

[53] We also find that the monthly mean AOT_{500} of the PCASP model is approximately 30% lower than the base model at Ndola. The high mean Ångström exponent (α = 1.66) of the PCASP model suggests that the size distribution results in a smaller fine mode median radius relative to the base model, but the lower mean curvature value suggests a greater relative contribution of coarse mode particles to the total AOT. When the column-integrated volume size distribution simulated by the PCASP model is compared to the base model at Ndola on 16 September, we find that the PCASP model has a smaller fine mode median radius relative to the base model, but a larger volume (mass) concentration at radius sizes between 1.00 and 10.00 μm, which explains the higher Ångström exponent (smaller fine mode) but lower optical depth and curvature term (more of the mass in the coarse mode). We also find that the PCASP model is roughly 20% more absorbing then the base model at both study sites.

[54] The monthly mean AOT_{500}, curvature term and SSA_{440} results from the AERONET-mean model were not significantly different from the base model results at Ndola (see Table 2). However, the mean Ångström exponent [380/440] of the AERONET-mean model is slightly higher than the base model suggesting that the AERONET-mean model has a slightly smaller fine mode median radius. Since the results from the AERONET-mean model are similar to the base model, suggests that the source and composition of particles on days assumed to be dominated by smoke does not change considerably from day to day.

[55] On a monthly basis, we find that using 22 size bins, compared to the 16 size bins used in the base model, does slightly impact the computed optical properties. We find that the monthly mean $\alpha_{380/440}$ of the 22-bin model is slightly lower and the curvature value is higher than the base model which has 16 size bins. These results are consistent with our 1-day comparisons (16 September 2000) discussed above. We also find that the monthly mean $\alpha_{380/440}$ of the 22-bin model is slightly lower and the curvature value is higher than the AERONET observations. These results suggest that the fine mode median radius is slightly too large in the model and slightly too much of the aerosol optical thickness is due to the fine mode fraction. This lack of large particles is further discussed below, where we show that the model does not produce the observed concentration of coarse mode particles.

[56] Overall, these results suggest that the transport of a size distribution and the appropriate bin resolution of the fine mode fraction in the model are important in order to obtain optical properties that are comparable to AERONET. The mass model produced mean AOT_{500} values that were higher and aerosols that were more absorbing than both the base model and the AERONET observations at the study sites. Additionally, the mass model has the disadvantage that it cannot capture the aging of the particles as they evolve over several days. *Westphal and Toon* [1991] and *Colarco et al.* [2004], among others, simulated the evolution of smoke plumes over several days and found that the aerosol optical properties changed as the particles evolved by coagulation.

4.2.2. Sensitivity to Aerosol Aging Processes

[57] The size of the aerosol is important when calculating the optical properties because different particle sizes scatter different amounts of radiation. Several observational studies have shown that aerosol size distributions shift toward larger sizes as the aerosol ages because of both coagulation and gas-to-particle conversion [*Reid et al.*, 1998; *Eck et al.*, 2001, 2003; *Haywood et al.*, 2003]. Simulations of smoke over multiday periods have also suggested that coagulation is necessary in order to explain the change in particle size distributions and optical properties as the smoke ages [*Westphal and Toon*, 1991; *Colarco et al.*, 2004]. In this section, we investigate the model's sensitivity to coagulation by conducting a simulation where the particles were not allowed to coagulate (referred to as the "no coagulation" in Tables 2 and 5).

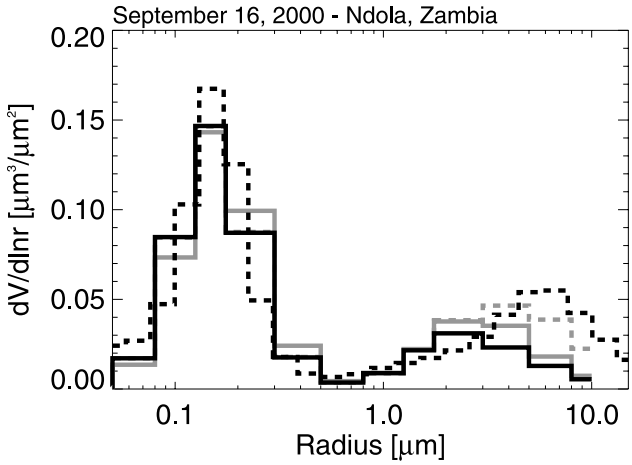

Figure 17. Normalized daily mean column-integrated AERONET and simulated volume size distributions at Ndola, Zambia, on 16 September 2000. The model size distributions are normalized to the fine volume concentration of the AERONET retrieval. The solid black line represents the base model, the gray line represents density model, the gray dashed line represents the no dry deposition model, and the dashed black line represents the AERONET retrieval.

[58] In our no coagulation simulation, we find that the mean AOT_{500} of smoke-dominated days is approximately 10% lower than the base model at Ndola. More significantly, without coagulation, the Ångström exponent is higher while the curvature term is lower relative to both the base model and the AERONET observations, suggesting that coagulation leads to a more realistic size distribution (Table 2). We also found that the computed SSA_{440} for the no coagulation model was slightly lower (i.e., more absorbing) than both the base model and the AERONET observation, although both the base and no coagulation models are within the uncertainty of the AERONET retrieval error bars. The interpretation of these results is complicated by the choice of initial particle size distribution and the resolution of the spectral optical properties in the base model. As found above, we may need more size bins than in the base model to resolve the fine mode fraction in order to observe coagulation evolve over this short period of time. Additionally, since the aging processes, particularly condensation, are reported to rapidly increase the particle size within the first 2 hours after emission near the smoke source [*Radke et al.*, 1995; *Reid et al.*, 1998], using a model with a coarse temporal resolution may make it difficult to monitor the initial aging processes of the smoke aerosols. However, capturing the initial aging process is not a goal of our study.

4.2.3. Sensitivity to Aerosol Removal Schemes

[59] As discussed previously in section 3.4, the model's volume concentration of particles greater than 2.00 μm are about a factor of 5 too low compared to AERONET and PCASP retrievals. The most likely model errors may be in our assumptions about the smoke aerosol properties (i.e., density and shape) and their relationship to our parameterizations of dry and wet removal processes that adversely affect the aerosol lifetimes.

[60] Currently, all of the smoke aerosols in the model have the same particle density (1.35 g cm^{-3} [*Reid et al.*, 1998]) and spherical shape. However, this may be a poor representation of the coarse mode particles which have been observed to be ash particles that could have a lower density and irregular shape. For these reasons, we conducted two additional simulations; one in which we decreased the particle density of the aerosols (referred to as "density" in Tables 2 and 5); and another in which we made the particles flat plates following the treatment prescribed by *Fuchs* [1964] (referred to as "shape" in Tables 2 and 5). Since there is no data reporting the density of ash particles released from biomass burning, we decreased the density by one half (0.675 g cm^{-3}). On the other hand, we may be using the appropriate smoke aerosol properties in the base model, however the dry deposition parameterization used to calculate the dry deposition velocities may be removing the aerosols in the model too vigorously. Therefore we conducted two additional simulations; one where we did not allow the aerosols to be removed by dry deposition and therefore eliminating both sedimentation and turbulent deposition (referred to as "no dry deposition" in Tables 2 and 5); and another where we implemented an alternative method to calculate the dry deposition velocities (referred to as "*Zhang et al.* [2001]" in Tables 2 and 5). The alternative dry deposition calculation we examined in this study follows the parameterization described by *Zhang et al.* [2001], which is more robust than the base model dry deposition routine by *Shao* [2000]. In particular, *Zhang et al.* [2001] consider surface type, where *Shao* [2000] does not.

[61] In general, we find that nonspherical particle shapes, low densities, and reduced dry deposition velocities improves the volume of the coarse mode fraction relative to AERONET (Figure 17). The fact that we are able to maintain the large particles by adjusting the input parameters in the model suggests that more information is needed about the actual particle shapes and densities. On the other hand, since the initial particle size distribution in the model may represent both local and transported aerosols, the coarse mode fraction of the transported aerosol may have been even more pronounced at the source. Thus the base model may not be initialized with enough coarse mode particles. Altogether, without more information about the properties of the smoke's coarse mode, we do not know which properties are the most appropriate to use in the model for coarse particles. Further investigation of the smoke coarse mode size distribution is a subject for future research.

[62] Of the tests conducted in this section thus far, we found that the simulated optical properties were significantly impacted by the change in particle density (Table 2). Since we want to maintain the same injected total particle mass, decreasing the particle density by half doubles the number of particles injected, which results in increasing both the rate of coagulation of fine mode particles and the computed AOT, but decreasing the computed Ångström exponent. The optical properties of the other tests in this section are essentially the same as the base model. The slightly lower curvature terms of these tests relative to the base model are due to the additional coarse mode particles each test provides.

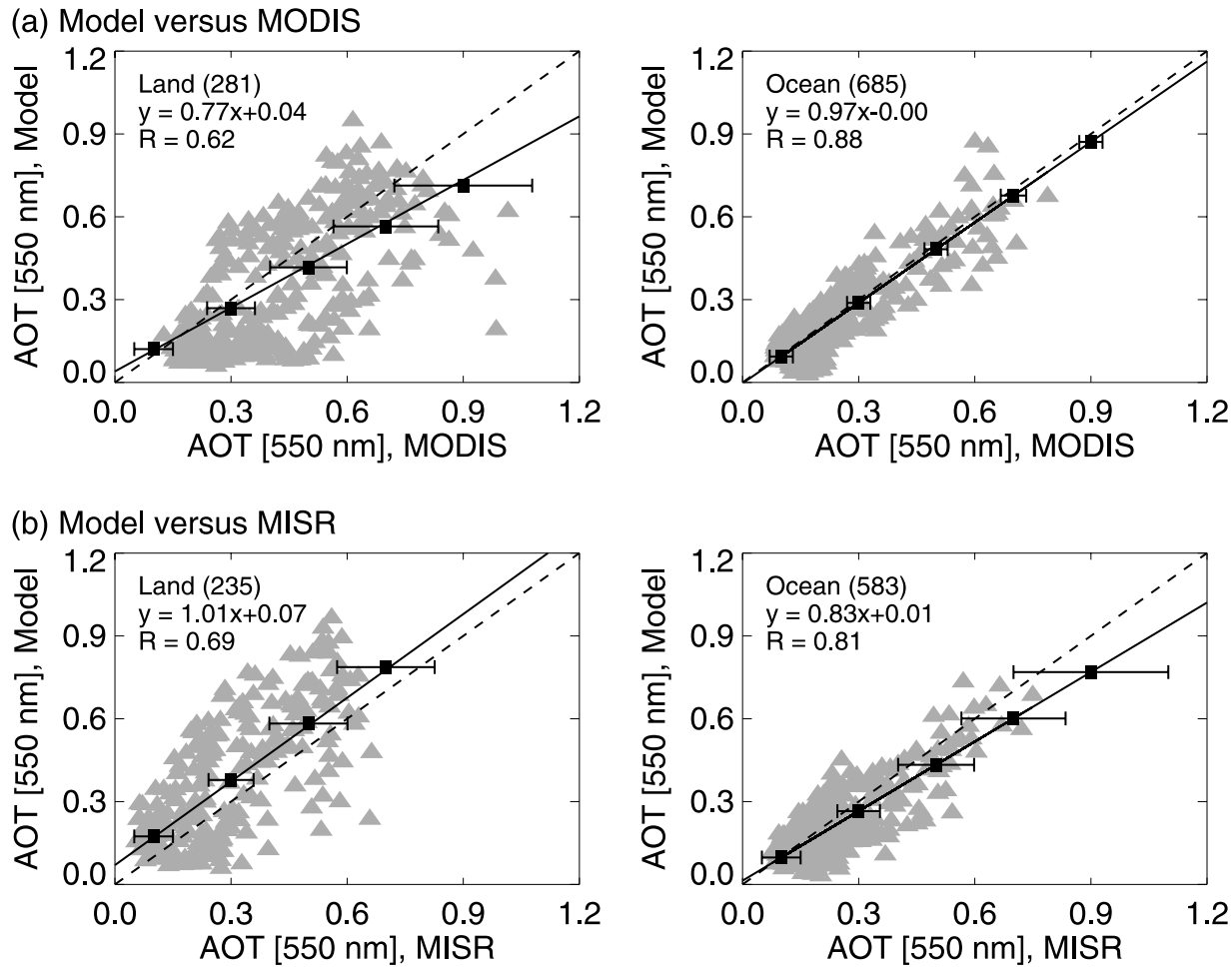

Figure 18. (a) Scatterplots of monthly mean AOT_{550} observed by MODIS versus the no removal model. (b) Scatterplots of monthly mean AOT_{550} observed by MISR versus the no removal model. The domain is divided into two regions: (left) land and (right) ocean (right). The dashed line represents the 1-to-1 line, and the solid black line represents the LBF. The equation of the LBF, the correlation coefficient (R), and the number of grid boxes (in parentheses) are reported.

[63] In this study, we also investigate the wet removal or "scavenging" parameterization used in the model. Briefly, the smoke aerosol is either affected by cumulus precipitation or stratiform precipitation and evaporation, and follows the treatment by *Barth et al.* [2000], which is independent of particle size. Briefly, in grid cells affected by cumulus precipitation, the smoke aerosols will be removed from the model. In grid cells affected by stratiform precipitation, the smoke aerosols swept up in a higher model layer may be removed entirely from the model or return to a lower layer where evaporation occurs. For below-cloud scavenging we assume a 10% efficiency [*Balkanski et al.*, 1993], while for in-cloud scavenging we assume that 100% of the aerosol present in the cloud fraction resides in the cloud water, and is removed in proportion to the rate of precipitation formation. Over southern Africa, the average rainfall in September is approximately 30 mm. Additionally, the monthly mean rainfall rate of about 1 mm day^{-1} is nearly uniform over southern Africa during September 2000. To test our wet removal scheme, we ran a simulation where the smoke aerosols were not allowed to be removed by scavenging (referred to as "no wet removal" in Tables 2 and 5).

[64] Figure 18 shows scatterplots of the monthly mean AOT_{550} retrieved by MODIS and MISR versus the no wet removal model. The domain is divided into the same two regions discussed above in section 3.3. In general, the simulated AOT_{550} increases by about 25% when we do not allow the smoke aerosols to be removed by rain over the land and ocean regions. In this case, the model results are within the error bars of the satellite data, and are essentially similar to a 25% increase in the smoke emissions. We also find that the monthly mean AOT_{500} simulated by the no wet removal model increases by 15% or less relative to the base model at Ndola and Inhaca (Figure 7 and Table 2). Since rain does occur over southern Africa, there is no justification for not including this removal process.

4.2.4. Sensitivity of Simulated Aerosol Properties to Optical Property Assumptions

[65] In this section we examine how different refractive index assumptions, including wavelength-dependent and wavelength-independent refractive indices (section 4.2.4.1),

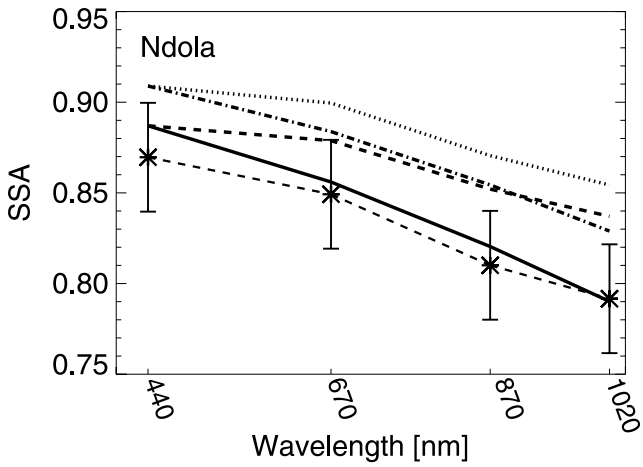

Figure 19. AERONET and simulated mean spectral dependence of SSA of smoke-dominated days for September 2000 at Ndola. The solid line represents the results from the base model, the dotted line represents the WD-AERONET model, the dashed-dotted line represents the WI-AERONET model, the dashed line represents the WD-AERONET-mean model, and the asterisks connected with dashed line represent the AERONET retrievals.

and the humidification of the smoke aerosol (section 4.2.4.2) affect the smoke aerosol optical properties.

4.2.4.1. Sensitivity to Smoke Refractive Index

[66] To examine the model's sensitivity to choice of refractive index, we tested four different refractive indices that are representative of biomass burning aerosols (Table 5). Note, in the base case we used a wavelength-independent refractive index, which represents the monthly mean refractive index at 440 nm retrieved by AERONET at Ndola, Zambia, during September 2000 ($N_{ref} = 1.51 - 0.024i$). This site was selected because of its proximity to smoke sources, suggesting that it was dominated by locally generated smoke aerosols. The refractive indices used in the sensitivity tests were either calculated by *Haywood et al.* [2003] or retrieved by AERONET. *Haywood et al.* [2003] calculated a refractive index of $1.54 - 0.025i$ at 550 nm for young smoke aerosols. This refractive index was applied to all wavelengths (wavelength-independent (WI)) and referred to as "WI–*Haywood et al.* [2003]" in Tables 2 and 5. We also selected a refractive index retrieved on 16 September 2000 at Ndola by AERONET ($N_{ref} = 1.52 - 0.019i$ at 440 nm). Again, we chose this particular day since it had the highest AOT_{500}, which suggests that this day was largely dominated by smoke aerosols. This refractive index was applied to all wavelengths (wavelength-independent) and referred to as "WI-AERONET" in Tables 2 and 5. We also explored wavelength-dependent (WD) refractive indices, which are listed in Tables 2 and 5. The "WD-AERONET" model applied refractive indices retrieved by AERONET on 16 September at 440, 670, 870, and 1020 nm, and the "WD-AERONET-mean" model applied the mean refractive indices of smoke-dominated days retrieved by AERONET at Ndola, Zambia, in September 2000 at the same wavelengths (Table 5).

[67] We find that the monthly mean AOT_{500} and $\alpha_{380/440}$ of smoke-dominated days are not sensitive to the choice of complex refractive index within the narrow range we considered in this study (Table 2). However, we did find that the simulated mean curvature values and wavelength dependence of SSA are sensitive to the choice of refractive index (see Table 2 and Figure 19). Since Inhaca has influences from other aerosol sources (i.e., dust and sea salt aerosols), we only present the results at Ndola. Compared to the base model, the WI models have higher curvature values, while the WD models have lower curvature values. Additionally, we find that the magnitude of the wavelength dependence of SSA of the refractive indices investigated here were higher than the base model (solid line) and in some cases outside the uncertainty of the AERONET retrievals (Figure 19). Overall, we find that the optical properties of the base model, which uses a wavelength-independent refractive index, are more comparable to the AERONET observations than the WD cases.

4.2.4.2. Sensitivity to the Humidification of the Smoke Aerosols

[68] To test the model's sensitivity to the humidification of the smoke aerosols, we considered a test where we assumed that the relative humidity at all locations was zero (referred to as "no hygroscopic growth" in Tables 2 and 5). Compared to the base model, we find that when we do not treat the humidification of aerosols or assume the smoke aerosols are completely dry, the mean AOT_{500} is lower and the aerosols become slightly more absorbing at Ndola. However, the Ångström exponent and curvature terms remain relatively unchanged (Table 2). Since the average relative humidity reported by MATCH at the selected study sites is 50% or less, we may not observe significant changes in the simulated optical properties when we treat the humidification of the smoke aerosols.

5. Summary

[69] In this study, we investigated the transport and optical properties of smoke aerosols produced from African biomass burning using a three-dimensional aerosol microphysical, transport, and radiation model. One of our goals in this study was to determine if we could use the data collected during the SAFARI 2000 field campaign as input parameters in our model to reproduce the observed optical properties. Our second goal was to better understand the parameters in our model that control the transport and optical properties of smoke aerosols. The principle findings of our study are summarized as follows:

[70] 1. In comparisons to AERONET AOT, we find that our model is able to reproduce most of the day-to-day variability in the AOT_{500} at the six AERONET sites investigated in this study. In general, we find that the model agrees well with the daily AOT_{500} retrievals from AERONET when the observed AOT_{500} is less than 1.00. When the AERONET AOT_{500} retrievals are greater than 1.00, the model underestimates the daily AOT_{500} by about 50%. In certain instances where the model significantly underestimated the aerosol loading with respect to AERONET, we found from satellite imagery that the model had slightly misplaced the smoke plume relative to the observations, suggesting possible errors in the model transport dynamics and/or the smoke emissions inventory during this time. At the six AERONET sites, the model under-

estimates the monthly mean AOT by 30% or less, suggesting either an uncertainty in the magnitude of the smoke emissions or the contributions from other aerosol species that we are not simulating in this study. Sensitivity tests in which we varied the diurnal emissions of the smoke or the timing of emissions throughout the month using daily satellite fire counts showed little effect on the daily variability of simulated AOT_{500}. These results suggest that the aerosol loading over the continent is most strongly controlled by transport dynamics, which is consistent with results from *Myhre et al.* [2003]. Given that the daily emissions data set generated in this study did not improve the day-to-day variability in the simulated AOT_{500} also suggests that simply using hot spots to scale the GFED emissions misses other important variables that determine the actual daily emissions.

[71] 2. In comparisons to satellite observations, we find that our model is capable of simulating smoke plume features similar to those observed by SeaWiFS, MODIS, and MISR over southern Africa and the Atlantic Ocean. Qualitatively, this suggests that the input parameters and microphysical processes in our model are adequate over a large region. Quantitatively, we find that the simulated monthly mean AOT_{550} is linearly correlated to the satellite observations, but the model is consistently lower than the satellite observations. The strong correlations between the model results and observations suggest that the differences do not represent random errors, but rather systematic errors. Over continental Africa, the simulated AOT_{550} is within the error bars of the MISR retrievals and about 20% lower than the MODIS retrievals. Over the ocean, the simulated AOT_{550} is about 40% and 30% lower than MISR and MODIS, respectively. The disagreement among the model and satellite observations may be a result of subpixel cloud contamination in the satellite retrievals, the contribution of other aerosol species that we are not simulating in our model, errors in the assumptions of the aerosol optical properties used in the satellite retrievals and in the model, or the monthly mean smoke emissions may be too low. The disagreement between MODIS and MISR over the land makes it difficult to quantify the model's monthly mean performance over continental Africa to better than about 30%.

[72] 3. In comparisons to airborne and ground-based measurements of extinction, the simulated vertical extinction profiles from our model compare favorably to the AATS-14, MPL, and CPL measurements. The minor differences found between the simulations and observations may be a result of the smoke injection function and the fact that we are using monthly mean smoke emissions. When exploring simulations with elevated smoke injections, we find that the base model, where the smoke is uniformly mixed throughout the depth of the PBL, provides results that are most comparable to the observations.

[73] 4. In comparisons of SSA, Ångström exponent, and mass optical efficiencies, the model compares fairly well to AERONET. We find that the average simulated Ångström exponent agrees well with the AERONET observations; however the model does not capture the daily variability in the Ångström exponent. It is likely that the observed fluctuations in the Ångström exponent are partly due to the diurnally varying contributions from other aerosol species that are not simulated in this study, and the variations in the age of the smoke aerosols. We also find that the simulated SSA is within the uncertainty of the AERONET SSA retrievals. Even though we assume a wavelength-independent refractive index in the simulated optical property calculations, the model produces wavelength-dependent results which compare well to the AERONET observations. Additionally, we find that the model's monthly mean mass scattering efficiency of fine mode particles over Africa is slightly higher than AERONET and other studies. However, the mass absorption efficiency is within the range of other studies.

[74] 5. In comparisons of particle microphysical properties, we find that the simulated Ångström exponent from the base model is within a few percent of those derived from the AERONET observations at the selected study sites. These results suggest that our particle size distributions, as modified by coagulation and relative humidity, are reasonable. However, the model underestimates the mass of coarse mode fraction relative to both AERONET and PCASP retrievals. Assuming that there is no error in the volume distribution of the coarse mode retrieved by AERONET and PCASP, these comparisons suggest that the model is removing these coarse mode particles too aggressively. The results from various sensitivity tests suggest that nonspherical shapes or lower density coarse mode particles would reduce the removal rate of the large particles. We also find that the simulated optical properties are sensitive to the choice of initial particle size distribution and to the number of size bins used to resolve the fine mode fraction of the particle size distribution. Sensitivity tests of the optical calculations further suggest that at least ten size bins are needed to adequately resolve the fine mode (i.e., radius sizes between 0.01 and 1.0 μm) optical properties.

[75] 6. When simulating smoke aerosols using a climate model, there are many sources of uncertainties. We find that the smoke source strength and time, transport, initial particle size distribution, injection altitude, particle properties (i.e., density and shape), and aging and removal processes will affect the amount and distribution of the aerosol mass. Additionally, the choice of refractive index or hygroscopic properties will impact the aerosol optics. Any uncertainty in these components will ultimately affect the model results and optical properties of the smoke aerosols. For example, the parameters used to estimate the smoke source, such as the emission factor and the burned area product, are highly uncertain. Therefore any errors in the smoke emissions will have a direct effect on the simulated AOT. In this study, we found that the combined uncertainties in the smoke source function (i.e., GFED carbon data set and emission factor) significantly impact the simulated AOT, where we observed a linear relationship between the smoke mass emitted and the simulated AOT. In order for the simulated AOT to be within the uncertainty of all the observations, the smoke emissions used in the base model must increase by about 30%. Furthermore, any uncertainties in the transport dynamics in the model may cause the smoke plumes to miss the point measurement sites. Alternatively, given the amount and distribution of the aerosol mass, a small error in the assumed refractive index will impact the simulated SSA and Ångström exponent.

[76] The satellite retrievals also make assumptions that can potentially produce large errors in the retrieved AOT. In order to derive the AOT from the measured radiance, assumptions about the surface reflectance, aerosol type, size distributions, complex refractive index, and cloud fraction are required [*Kaufman et al.*, 1997; *Tanré et al.*, 1997; *Diner et al.*, 1998; *Martonchik et al.*, 1998]. Therefore any differences in the assumptions applied in the retrieval algorithms raise the level of uncertainty. One of the largest known problems in the satellite retrievals are cloud-contaminated pixels. It is difficult to screen thin clouds, however these unfiltered clouds pose problems that can lead to an overestimated AOT.

[77] Since the AERONET retrievals provide an extensive network of multiple aerosol optical property measurements (i.e., AOT, SSA, Ångström Exponent, Particle Size Distribution, and Refractive Index), they are important for instrument and model validation. However, the AERONET data carry some uncertainties given the fact that they are only point measurements retrieved during the daytime under cloud-free conditions. Here the point measurements may not be representative of the model grid box which in our case about 200 km $\times$ 200 km. Additionally, the AERONET data assume that the aerosol particles are homogeneous spheres which can affect the retrieved particle properties.

[78] Given the uncertainties in the simulated smoke aerosols and observations, the last obstacle arises from properly making the intercomparisons between the model results and observations. Unfortunately, it is difficult to compare our model results to the observations in a consistent manner since they have different temporal and spatial resolutions, and are based on different physical and optical property assumptions. As suggested above, we provided a means to quantitatively compare the model results to the observations, however more work needs to be done to investigate our aggregation and sampling technique used for the satellite data. Additionally, we find that the AERONET and satellite observations do not frequently overlap in time at a single location. Subsequently, this makes it difficult to compare the model results at a single location to more than one instrument at a given time.

[79] Overall, we find that we can use the data sets available in the scientific community to reproduce the observed smoke aerosol optical properties on a monthly basis with very good fidelity. In doing so, we have developed a set of measurement-based initial conditions to specify the aerosol emissions, injection altitude, and particle size distribution in climate models to simulate the smoke plumes originating over southern Africa. This work is a step toward improved quantification of smoke aerosol optical properties for use in calculating the direct effects of these aerosols on climate, and provides a strategy for the incorporation of particle size distributions into microphysical models attempting to simulate the aging of smoke aerosols. However, we did find inconsistencies in the AOT comparisons over continental Africa among AERONET, MISR, and MODIS data that need to be better understood in order for us to feel confident in using them to assess the performance of our model.

[80] **Acknowledgments.** This work was supported by NSF-ATM0435713 and NIP/03-0000-0043. Rebecca Matichuk was partially supported by the NASA Goddard GSRP program. We would like to thank the following people and groups for kindly providing data and assisting us with the satellite, aircraft, and ground-based data used in our study: B. N. Holben (AERONET data), R. Kahn (MISR data), R. Levy (MODIS data), O. Torres (EP-TOMS data), M. McGill and D. Hlavka (CPL), B. Schmidt (AATS-14 measurements), J. Spinhirne and NASA Earth Observatory System (MPL data), G. van der Werf (GFED data), S. Korontzi (Smoke Emissions), and L. Zhang (Dry Deposition Routine). We would also like to thank the reviewers for their time, thoughtful comments, and suggestions.

References

Ackerman, A., O. Toon, and P. Hobbs (1995), A model for particle microphysics, turbulent mixing, and radiative-transfer in the stratocumulus-topped marine boundary-layer and comparisons with measurements, *J. Atmos. Science*, *52*, 1204–1236.

Andreae, M. O., and P. Merlet (2001), Emission of trace gases and aerosols from biomass burning, *Global Biogeochem. Cycles*, *15*, 955–966.

Annegarn, H. J., L. Otter, R. Swap, and R. Scholes (2002), Southern Africa's ecosystem in a test-tube–A perspective on the Southern African Regional Science Initiative (SAFARI 2000), *S. Afr. J. Sci.*, *98*, 111–113.

Arino, O., A. Buongiorno, and P. Goryl (1995), Intercalibration of AVHRR and ATSR data, *Adv. Space Res.*, *17*(1), 29–38.

Balkanski, Y., D. Jacob, G. Gardner, W. Grausten, and K. Turekian (1993), Transport and residence times of tropospheric aerosols inferred from a global three-dimensional simulation of ^{210}Pb, *J. Geophys. Res.*, *98*, 20,573–20,586.

Barth, M. C., P. J. Rasch, J. T. Kiehl, C. M. Benkovitz, and S. E. Schwartz (2000), Sulfur chemistry in the National Center for Atmospheric Research Community Climate Model: Description, evaluation, features, and sensitivity to aqueous chemistry, *J. Geophys. Res.*, *105*, 1387–1416.

Chin, M., P. Ginoux, S. Kinne, O. Torres, B. Holben, B. Duncan, R. Martin, J. Logan, A. Higurashi, and T. Nakajima (2002), Tropospheric aerosol optical thickness from the GOCART model and comparisons with satellite and sun photometer measurements, *J. Atmos. Science*, *59*, 461–483.

Colarco, P. R., O. B. Toon, O. Torres, and P. J. Rasch (2002), Determining the UV imaginary index of refraction of Saharan dust particles from Total Ozone Mapping Spectrometer data using a three-dimensional model of dust transport, *J. Geophys. Res.*, *107*(D16), 4289, doi:10.1029/2001JD000903.

Colarco, P. R., O. B. Toon, and B. N. Holben (2003a), Saharan dust transport to the Caribbean during PRIDE: 1. Influence of dust sources and removal mechanisms on the timing and magnitude of downwind aerosol optical depth events from simulations of in situ and remote sensing observations, *J. Geophys. Res.*, *108*(D19), 8589, doi:10.1029/2002JD002658.

Colarco, P. R., et al. (2003b), Saharan dust transport to the Caribbean during PRIDE: 2. Transport, vertical profiles, and deposition in simulations of in situ and remote sensing observations, *J. Geophys. Res.*, *108*(D19), 8590, doi:10.1029/2002JD002659.

Colarco, P. R., M. R. Schoeberl, B. G. Doddridge, L. T. Marufu, O. Torres, and E. J. Welton (2004), Transport of smoke from Canadian forest fires to the surface near Washington, D.C.: Injection height, entrainment, and optical properties, *J. Geophys. Res.*, *109*, D06203, doi:10.1029/2003JD004248.

Crutzen, O. J., and M. O. Andreae (1990), Biomass burning in the tropics–Impact on atmospheric chemistry and biogeochemical cycles, *Science*, *250*, 1669–1678.

Diner, D. J., et al. (1998), Multiangle imaging spectroradiometer (MISR) instrument description and experiment overview, *IEEE Trans. Geosci. Remote Sens.*, *36*, 1072–1087.

Dubovik, O., and M. D. King (2000), A flexible inversion algorithm for retrieval of aerosol optical properties from Sun and sky radiance measurements, *J. Geophys. Res.*, *105*, 20,673–20,696.

Eck, T. F., B. N. Holben, J. S. Reid, O. Dubovik, A. Smirnov, N. T. O'Neill, I. Slutsker, and S. Kinne (1999), Wavelength dependence of the optical depth of biomass burning, urban, and desert dust aerosols, *J. Geophys. Res.*, *104*, 31,333–31,350.

Eck, T. F., B. N. Holben, D. E. Ward, O. Dubovik, J. S. Reid, A. Smirnov, M. M. Mukelabai, N. C. Hsu, N. T. O'Neill, and I. Slutsker (2001), Characterization of the optical properties of biomass burning aerosols in Zambia during the 1997 ZIBBEE field campaign, *J. Geophys. Res.*, *106*, 3425–3448.

Eck, T. F., et al. (2003), Variability of biomass burning aerosol optical characteristics in southern Africa during the SAFARI 2000 dry season campaign and a comparison of single scattering albedo estimates from radiometric measurements, *J. Geophys. Res.*, *108*(D13), 8477, doi:10.1029/2002JD002321.

Formenti, P., W. Elbert, W. Maenhaut, J. Haywood, S. Osborne, and M. Andreae (2003), Inorganic and carbonaceous aerosols during the Southern African Regional Science Initiative (SAFARI 2000) experiment:

Chemical characteristics, physical properties, and emission data for smoke from African biomass burning, *J. Geophys. Res.*, *108*(D13), 8488, doi:10.1029/2002JD002408.

Fuchs, N. A. (1964), *The Mechanics of Aerosols*, Dover, Mineola, N. Y.

Giglio, L., J. D. Kendall, and R. Mack (2003), A multi-year active fire data set for the tropics derived from the TRMM VIRS, *Int. J. Remote Sens.*, *24*, 4505–4525.

Hao, W. M., M. H. Liu, and P. J. Crutzen (1990), Estimates of annual and regional releases of CO_2 and their trace gases to the atmosphere from fires in the tropics, based on the FAO statistics for the period 1975–1980, in *Fire in the Tropical Biota: Ecosystem Processes and Global Challenges*, *Ecol. Studies 84*, edited by J. G. Goldammer, pp. 440–462, Springer, New York.

Haywood, J. M., S. R. Osborne, P. N. Francis, A. Keil, P. Formenti, M. O. Andreae, and P. H. Kaye (2003), The mean physical and optical properties of regional haze dominated by biomass burning aerosol measured from the C-130 aircraft during SAFARI 2000, *J. Geophys. Res.*, *108*(D13), 8473, doi:10.1029/2002JD002226.

Holben, B. N., et al. (1998), AERONET–A federated instrument network and data archive for aerosol characterization, *Remote Sens. Environ.*, *66*, 1–16.

Ichoku, C., L. A. Remer, Y. J. Kaufman, R. Levy, D. A. Chu, D. Tanré, and B. N. Holben (2003), MODIS observation of aerosols and estimation of aerosol radiative forcing over southern Africa during SAFARI 2000, *J. Geophys. Res.*, *108*(D13), 8499, doi:10.1029/2002JD002366.

Intergovernmental Panel on Climate Change (2001), *Climate Change 2001: The Scientific Basis: Contribution of Working Group I to the Third Assessment Report of the Intergovernmental Panel on Climate Change*, edited by J. T. Houghton et al., 881 pp., Cambridge Univ. Press, New York.

Kalnay, E., et al. (1996), The NCEP/NCAR 40-year reanalysis project, *Bull. Am. Meteorol. Soc.*, *77*, 437–471.

Kaufman, Y. J., D. Tanré, L. A. Remer, E. F. Vermote, A. Chu, and B. N. Holben (1997), Operational remote sensing of tropospheric aerosol over land from EOS moderate resolution imaging spectroradiometer, *J. Geophys. Res.*, *102*, 17,051–17,068.

Li, Y., T. H. Demetriades-Shah, E. T. Kanemasu, J. K. Shultis, and M. Kirkam (1993), Use of second derivatives of canopy reflectance for monitoring prairie vegetation over different soil backgrounds, *Remote Sens. Environ.*, *44*, 81–87.

Lin, S. J., and R. B. Rood (1996), Multidimensional flux-form semi-Lagrangian transport schemes, *Mon. Weather Rev.*, *124*, 2046–2070.

Magi, B. I., and P. V. Hobbs (2003), Effects of humidity on aerosols in southern Africa during the biomass burning season, *J. Geophys. Res.*, *108*(D13), 8495, doi:10.1029/2002JD002144.

Martonchik, J., D. Diner, R. Kahn, T. Ackerman, M. Verstraete, B. Pinty, and H. Gordon (1998), Techniques for the retrieval of aerosol properties over land and ocean using multiangle imaging, *IEEE Trans. Geosci. Remote Sens.*, *36*, 1212–1227.

McGill, M. J., D. L. Hlavka, W. D. Hart, E. J. Welton, and J. R. Campbell (2003), Airborne lidar measurements of aerosol optical properties during SAFARI-2000, *J. Geophys. Res.*, *108*(D13), 8493, doi:10.1029/2002JD002370.

Myhre, G., T. K. Berntsen, J. M. Haywood, J. K. Sundet, B. N. Holben, M. Johnsrud, and F. Stordal (2003), Modeling the solar radiative impact of aerosols from biomass burning during the Southern African Regional Science Initiative (SAFARI-2000) experiment, *J. Geophys. Res.*, *108*(D13), 8501, doi:10.1029/2002JD002313.

O'Neill, N. T., T. F. Eck, B. N. Holben, A. Smirnov, A. Royer, and Z. Li (2002), Optical properties of boreal forest fire smoke derived from Sun photometry, *J. Geophys. Res.*, *107*(D11), 4125, doi:10.1029/2001JD000877.

Pruppacher, H. R., and J. D. Klett (1997), *Microphysics of Clouds and Precipitation*, Springer, New York.

Radke, L. F., D. Hegg, P. Hobbs, and J. Penner (1995), Effects of aging on the smoke from a large forest fire, *Atmos. Res.*, *38*, 315–332.

Rasch, P. J., N. M. Mahowald, and B. E. Eaton (1997), Representations of transport, convection, and the hydrologic cycle in chemical transport models: Implications for the modeling of short-lived and soluble species, *J. Geophys. Res.*, *102*, 28,127–28,138.

Reid, J. S., P. V. Hobbs, R. J. Ferek, D. R. Blake, J. V. Martins, M. R. Dunlap, and C. Liousse (1998), Physical, chemical, and optical properties of regional hazes dominated by smoke in Brazil, *J. Geophys. Res.*, *103*, 32,059–32,080.

Reid, J., R. Koppmann, T. Eck, and D. Eleuterio (2004a), A review of biomass burning emissions, part II: Intensive physical properties of biomass burning particles, *Atmos. Chem. Phys. Disc.*, *4*, 5135–5200.

Reid, J., T. Eck, S. Christopher, R. Koppmann, O. Dubovik, D. Eleuterio, B. Holben, E. Reid, and J. Zhang (2004b), A review of biomass burning emissions, part III: Intensive optical properties of biomass burning particles, *Atmos. Chem. Phys. Disc.*, *4*, 5201–5260.

Schmid, B., et al. (2003), Coordinated airborne, spaceborne, and ground-based measurements of massive thick aerosol layers during the dry season in southern Africa, *J. Geophys. Res.*, *108*(D13), 8496, doi:10.1029/2002JD002297.

Scholes, M., and M. O. Andreae (2000), Biogenic and pyrogenic emissions from Africa and their impact on the global atmosphere, *Ambio*, *29*, 23–29.

Shao, Y. (2000), *Physics and Modeling of Wind Erosion*, Springer, New York.

Sinha, P., P. V. Hobbs, R. J. Yokelson, I. T. Bertschi, D. R. Blake, I. J. Simpson, S. Gao, T. W. Kirchstetter, and T. Novakov (2003), Emissions of trace gases and particles from savanna fires in southern Africa, *J. Geophys. Res.*, *108*(D13), 8487, doi:10.1029/2002JD002325.

Smirnov, A., B. N. Holben, T. F. Eck, O. Dubovik, and I. Slutsker (2000), Cloud screening and quality control algorithms for the AERONET database, *Remote Sens. Environ.*, *73*, 337–349.

Spinhirne, J. D., J. Rall, and V. S. Scott (1995), Compact eye safe lidar systems, *Rev. Laser, Eng.*, *23*, 112–118.

Stein, D. C., R. J. Swap, S. Greco, S. J. Piketh, S. A. Macko, B. G. Doddridge, T. Elias, and R. T. Bruintjes (2003), Haze layer characterization and associated meteorological controls along the eastern coastal region of southern Africa, *J. Geophys. Res.*, *108*(D13), 8506, doi:10.1029/2002JD003237.

Swap, R. J., H. J. Annegarn, J. T. Suttles, M. D. King, S. Platnick, J. L. Privette, and R. J. Scholes (2003), Africa burning: A thematic analysis of the Southern African Regional Science Initiative (SAFARI 2000), *J. Geophys. Res.*, *108*(D13), 8465, doi:10.1029/2003JD003747.

Tanré, D., Y. J. Kaufman, M. Herman, and S. Mattoo (1997), Remote sensing of aerosol properties over oceans using the MODIS/EOS spectral radiances, *J. Geophys. Res.*, *102*, 11,201–11,218.

Toon, O. B., R. Turco, D. Westphal, R. Malone, and M. Liu (1988), A multidimensional model for aerosols: Description of computational analogs, *J. Atmos. Sci.*, *45*, 2123–2144.

Torres, O., P. K. Bhartia, J. R. Herman, Z. Ahmad, and J. Gleason (1998), Derivation of aerosol properties from satellite measurements of backscattered ultraviolet radiation: Theoretical basis, *J. Geophys. Res.*, *103*(D14), 17,099–17,110.

Torres, O., P. Bhartia, A. Sinyuk, E. Welton, and B. Holben (2005), Total Ozone Mapping Spectrometer measurements of aerosol absorption from space: Comparison to SAFARI 2000 ground-based observations, *J. Geophys. Res.*, *110*, D10S18, doi:10.1029/2004JD004611.

van der Werf, G. R., J. T. Randerson, J. Collatz, and L. Giglios (2003), Carbon emissions from fires in tropical and subtropical ecosystems, *Global Change Biol.*, *9*, 547–562.

Warner, J., and S. Twomey (1967), The production of cloud nuclei by cane fires and the effect on cloud drop concentrations, *J. Atmos. Sci.*, *24*, 704–706.

Westphal, D. L., and O. B. Toon (1991), Simulations of microphysical, radiative, and dynamical processes in a continental-scale forest fire smoke plume, *J. Geophys. Res.*, *96*, 22,379–22,400.

Wiscombe, W. (1979), Mie scattering calculations: Advances in technique and fast, vector-speed computer codes, *NCAR Tech. Note TN-140+STR.*, Natl. Cent. for Atmos. Res., Boulder, Colo.

Zhang, L., S. Gong, J. Padro, and L. Barrie (2001), A size-segregated particle dry deposition scheme for an atmospheric aerosol module, *Atmos. Environ.*, *35*, 549–560.

P. R. Colarco, NASA Goddard Space Flight Center, Code 613.3, Greenbelt, MD 20771, USA.

R. I. Matichuk, J. A. Smith, and O. B. Toon, Laboratory for Atmospheric and Space Physics, Department of Atmospheric and Oceanic Sciences, University of Colorado, Boulder, CO 80309, USA. (rebecca.matichuk@lasp.colorado.edu)